



UNIVERSITY OF LEEDS

This is a repository copy of *Nanocellulose dissolution in green solvents: Enhancing carrageenan biocomposites for sustainable hard capsule production*.

White Rose Research Online URL for this paper:

<https://eprints.whiterose.ac.uk/225362/>

Version: Accepted Version

---

**Article:**

Okwuwa, C.C., Adam, F. and Ries, M.E. [orcid.org/0000-0002-8050-3200](https://orcid.org/0000-0002-8050-3200) (2025)

Nanocellulose dissolution in green solvents: Enhancing carrageenan biocomposites for sustainable hard capsule production. *Cellulose*. ISSN 0969-0239

<https://doi.org/10.1007/s10570-025-06474-2>

---

**Reuse**

This article is distributed under the terms of the Creative Commons Attribution (CC BY) licence. This licence allows you to distribute, remix, tweak, and build upon the work, even commercially, as long as you credit the authors for the original work. More information and the full terms of the licence here:

<https://creativecommons.org/licenses/>

**Takedown**

If you consider content in White Rose Research Online to be in breach of UK law, please notify us by emailing [eprints@whiterose.ac.uk](mailto:eprints@whiterose.ac.uk) including the URL of the record and the reason for the withdrawal request.



[eprints@whiterose.ac.uk](mailto:eprints@whiterose.ac.uk)  
<https://eprints.whiterose.ac.uk/>

# Nanocellulose Dissolution in Green Solvents: Enhancing Carrageenan Biocomposites for Sustainable Hard Capsule Production

Chigozie Charity Okwuwa<sup>1</sup>, Fatmawati Adam<sup>1,2\*</sup>, and Michael E. Ries<sup>3</sup>

<sup>1</sup>Faculty of Chemical and Process Engineering and Technology, Universiti Malaysia Pahang Al-Sultan Abdullah, Lebuhr Persiaran Tun Khalil Yaakob, 26300 Kuantan, Pahang, Malaysia.

<sup>2</sup>Centre for Research in Advanced Fluid and Processes, Universiti Malaysia Pahang Al-Sultan Abdullah, Kuantan, Pahang, Malaysia.

<sup>3</sup>School of Physics & Astronomy, University of Leeds, Leeds, LS2 9JT, United Kingdom.

Corresponding author: Faculty of Chemical and Process Engineering Technology, Universiti Malaysia Pahang Al-Sultan Abdullah, 26300 Kuantan, Pahang, Malaysia.

Email: fatmawati@ump.edu.my

**Abstract:** This study investigates the dissolution of nanocellulose in a green choline chloride glycerol-based deep eutectic solvent (DES) to enhance the performance of carrageenan biocomposites for pharmaceutical applications. It is hypothesized that varying the hydrogen bond donor (HBD) ratio (glycerol) of the DES from 1:1 to 1:4 significantly enhanced the dissolution of nanocellulose, which is critical for improving the properties of the resulting biocomposite. Structural analyses showed that the optimal HBD ratio of the DES maximized nanocellulose dissolution, confirmed by X-ray Diffraction (XRD) and Nuclear Magnetic Resonance (NMR) spectroscopy, which demonstrated structural modifications and hydrogen bond breakdown. Thermal analysis indicated that the reinforced carrageenan biocomposite film and hard capsules exhibited enhanced thermal stability, with a higher degradation temperature of 245 °C and improved mechanical strength, as well as high tensile strength and capsule loop strength. It is suggested that the dissolution mechanism involves the disruption of hydrogen bonds in cellulose crystalline structure by the HBD in DES and promotes uniform integration within the carrageenan matrix. By tailoring DES composition to achieve dissolution and performance characteristics in industrial applications, this study offers a green and sustainable approach to enhance the functional properties of carrageenan biocomposites, advancing their potential use in environmentally friendly and high-performance pharmaceutical materials.

**Keywords:** Cellulose Dissolution; Hydrogen Bond; Deep Eutectic Solvent; Carrageenan; Hard Capsules

## 1. Introduction

Carrageenan, which is a versatile natural polysaccharide extracted from red seaweed, primarily belonging to the Rhodophyceae family, has become a valuable ingredient in the food, pharmaceutical, and cosmetic industries due to its unique ability to form gels, thicken solutions, and stabilize emulsions (Nguyen et al., 2022). Carrageenan faces limitations that restrict its widespread use in the pharmaceutical industry (Pacheco-Quito et al., 2020). Current carrageenan-based hard capsules have low mechanical strength, thermal stability, and brittleness due to their double-helical molecular structure, limiting their industrial viability (Fauzi et al., 2021). Also, the surface roughness of carrageenan-based capsules falls short of industry standards, affecting their industrial viability (Li et al., 2014). Incorporating cellulose nanocrystal (CNC) into the matrix has shown promise as a reinforcing agent. However, CNCs present challenges, including their insolubility in water due to strong hydrogen bonds in their crystalline regions (Babaei-Ghazvini et al., 2024); these hydrogen bonds are also present in the amorphous zones but to a lesser extent. However, amorphous cellulose is also insoluble in water (Acharya et al., 2021; Gundupalli et al., 2023; Sirviö et al., 2019; Walters et al., 2020). This causes poor dispersion and weakens the mechanical properties and aesthetics of the hard capsules. In order to address these challenges, traditional solvents were used for cellulose dissolution, they are associated with health, safety, and environmental hazards, rendering them unsuitable for pharmaceutical applications (Okwuwa et al., 2023). Also, the use of ionic liquids, which is considered a green solvent for extracting and processing nanocellulose, often involves the use high processing costs (Kim et al., 2022; Xu & Wang, 2020) for the removal of toxic components of the ILs which causes environmental health risks due to their non-biodegradability and hazardous nature (Chen & Mu, 2021; Hawkins et al., 2021; Sulthan et al., 2023). This has spurred an urgent need for the development of greener and more sustainable solvent systems that can effectively dissolve cellulose without causing environmental harm (Cao & Su, 2021; Li et al., 2021; Liang et al., 2023; Nguyen et al., 2020; Yu et al., 2023).

DESs, which are made up of HBD and HBA, interact to form a homogenous mixture and have a melting point significantly lesser than that of the individual components (Jha et al., 2023; Jiang et al., 2020; Lomba et al., 2021) have emerged as a novel and

promising class of green solvents. HBDs are integral components of DESs, which provide the hydrogen atoms necessary for hydrogen bonding with HBAs. Common HBDs used in DESs include urea, glycerol, ethylene glycol, carboxylic acids, and sugars (Lomba et al., 2021). These molecules typically possess hydrogen atoms bound to electronegative atoms such as oxygen or nitrogen, enabling them to participate in hydrogen bonding interactions (S. Kim et al., 2024). The choice of HBD significantly influences the physical and chemical properties of DESs. For instance, urea-based DESs are known for their low viscosity and high conductivity, making them suitable for electrochemical applications (Cruz et al., 2020). Glycerol-based DESs, on the other hand, exhibit higher viscosity and enhanced solvation capacity, making them ideal for biomass processing and pharmaceutical applications (Zhang et al., 2012). The versatility of HBDs allows for the customization of DES properties to meet specific application requirements, from solubility and viscosity to thermal stability and reactivity. HBAs in DESs typically consist of quaternary ammonium salts such as choline chloride, tetrabutylammonium bromide, or metal halides like zinc chloride (Omar & Sadeghi, 2023). Choline chloride and glycerol used in this study form an edible DES and have gained significant attention due to its biocompatibility, low toxicity, and environmentally friendly nature (Li et al., 2024). Choline chloride, a quaternary ammonium salt, is widely recognized for its safety and is commonly used in food and pharmaceutical formulations (Gaioto et al., 2023). Similarly, glycerol, a polyol, is a food-grade compound often utilized as a humectant, sweetener, and solvent in various edible products (Goyal et al., 2021). Combining these two components creates a DES with unique physicochemical properties, such as a high hydrogen-bonding capacity and low volatility, making it suitable for applications in the pharmaceutical and food industries. From the studies of Wei et al. (2023), it has been demonstrated that such DES formulations are safe for human consumption and exhibit excellent solubilization capabilities for bioactive compounds, further enhancing their applicability. DESs have low toxicity, biodegradability, and ease of preparation (Farooq et al., 2020; Gomez et al., 2018; Pelosi et al., 2023; Tong et al., 2023; Q. Zhang et al., 2012), which aligns well with the principles of green chemistry and sustainable development (Omar & Sadeghi, 2022). The choline chloride-glycerol-based DES is particularly notable for dissolving polysaccharides such as cellulose, thereby providing a sustainable alternative to conventional solvents (Ramli et al., 2024a). The amino acid-based DES (AADES) and therapeutic DES (THEDES) are also used in pharmaceutical industries (Jadhav et al., 2021). The use of DES to enhance cellulose nanocrystal (CNC) dispersion was seen as the zeta potential increased by 43.2% and improved crystallinity from 76% to 81%, which boosted the capsule loop and tensile strength

of Carra-CNCDES by 19.4% and 20.7%, respectively, as well reducing surface roughness by 21.8% due to an optimized H-bond network (Ramli et al., 2024a). Feng et al. first oxidized cellulose into dialdehyde cellulose before dissolving in DES (Marchel et al., 2022).

The interaction mechanisms for the dissolution of cellulose in DES involve the availability of a hydrogen bond donor from DES, which weakens the intermolecular and intramolecular hydrogen bonds in cellulose, thus enhancing its dissolution. Factors such as the molar ratio of DES components, temperature, and the nature of HBD significantly influence the dissolution capacity (Feng et al., 2022). For instance, increasing the temperature typically enhances dissolution by reducing the viscosity of DES and increasing the mobility of cellulose chains (Jančíková & Jablonský, 2022). Moreover, DES can dissolve cellulose with varying degrees of polymerization and crystallinity (Altinkaya, 2024). The potential applications of cellulose dissolved in DES are vast, from textiles and bioplastics to pharmaceuticals and food packaging (Nam et al., 2023). This study systematically investigated the mechanisms underlying the dissolution of CNC in the DES by varying the HBD of the DES. CNC dissolved in DES-enhanced carrageenan biocomposite for producing hard capsules. The chemical interactions and shifting of the DES in the spectrum and their behaviour upon adding CNCs were analyzed using  $^1\text{H}$  NMR spectroscopy. SEM was utilized to examine the surface morphology of the reinforced carrageenan biocomposite films, providing insights into structural changes and surface characteristics. XRD analysis also identified CNC's crystalline and amorphous forms when dissolved in DES. The DSC and TGA were used to investigate the weight loss of the Carra-CNCDES films. These analyses provided insights into the thermal properties and stability of the films.

## **2. Experimental Section**

### **2.1. Materials and Chemicals**

Choline chloride (98%,  $139.62 \text{ g}\cdot\text{mol}^{-1}$ ), Glycerol (anhydrous, 99.9%, Aldrich), microcrystalline cellulose (Avicel PH-101), HPMC (average molecular weight of 86 kDa), 4-methoxybenzyl alcohol (98%) (anise), and calcium alginic acid (alg), these constituents were purchased from Sigma-Aldrich, USA. Refined carrageenan was purchased from CV Simpul Agro Globalindo, Indonesia (molecular weight ranges from 930 to 1010 g/mol) with 31.5% carbon, 5.97% hydrogen, 0% nitrogen, and 6.28% sulphur. A Milli-Q water system (Bedford, MA, USA) was used to prepare deionized water, and all chemicals were analyzed.

## **2.2. Preparation of DES**

Choline chloride (ChCl) underwent pretreatment to remove any potential moisture by being dried in a vacuum oven overnight at 80 °C before being used (Ramli et al., 2024), the dried ChCl was combined with glycerol by varying the HBD ratios from 1:1 to 1:4 and at a temperature of 60 °C; this was continuously stirred at each molar ratio to obtain a homogeneous mixture with no evidence of solid particles (Zhang et al., 2020). The eutectic mixture formed was kept as the DES.

## **2.3. Preparation for CNC**

5 g of microcrystalline cellulose (MCC) was dispersed in 500 ml of deionized water using a magnetic stir bar and left overnight to ensure thorough mixing. The resulting aqueous dispersion underwent ultrasonication for 50 minutes at 500 W power, 20 kHz frequency, and 20% amplitude using a QSonica ultrasonicator. After ultrasonication, the dispersion was allowed to settle undisturbed for a day. This process formed two distinct layers, with the upper layer predominantly consisting of evenly dispersed CNCs. Subsequently, the upper layer, identified as CNCs, was separated by decantation and subjected to freeze-drying for preservation and further analysis. (Mohd Amin et al., 2015), 0.2 g of the CNC was used in each sample preparation.

## **2.4. Dissolution of CNC in DES**

0.2 g of CNC was gradually added to 10 g of DES in a flask under mechanical stirring at 60°C for 24 hours, and 50 mL of DI water was added, forming two layers. The upper layer was decanted, while the lower precipitates (undissolved cellulose) were collected, weighed, and recorded as M (B. Cao et al., 2016). These residues were dried in a vacuum oven at 60°C until a constant weight was attained, called the regenerated CNC.

## **2.5. Preparation of Carrageenan Biocomposite Films and Hard Capsules**

0.2g of CNC was added to 10 g of DES solution and continuously stirred overnight; only 2 ml from the solution was used in each sample formulation, known as CNCDES (Ramli et al., 2024). Then, 3g of refined carrageenan was mixed in 60 ml of deionized water using a

mechanical stirrer at 60 °C and 200 rpm. The exact amount of hydroxypropyl methylcellulose (HPMC, 1 g), 4-methoxybenzyl alcohol (0.5 ml), and calcium alginate acid (0.07 g). was then added into the formulation as a thickener, crosslinker, and toughening agent, respectively (Ramli et al., 2024). 0.2 g of CNC was dissolved in 10 g of ChCl Gly-based DES at various ratios, 2 ml of this solution was incorporated into the carrageenan biocomposite, and the glycerol in the DES also served as a plasticizer. The differences in CNC characteristics result from the different HBA and HBD ratio combinations. Approximately 20 ml of the mixture biocomposite was poured into a stainless-steel tray with a diameter of 20 cm after five h of mixing. It was oven-dried at the temperature to form a film. Afterwards, dried biocomposite films were used for characterization and analysis (Hamdan et al., 2020). The formulation solution from preparing the carrageenan biocomposite was added to the deep stainless-steel mould, where the capsule pins of size “1” were dipped into the biocomposite to prepare hard capsules. Afterwards, dried biocomposite hard capsules were used for characterization and analysis (Kalmer et al., 2023).

## 2.6. Testing and Characterization

### i. FTIR Analysis of DES and CNC dissolved in DES

The identification of various functional groups present in the varied ratio of the HBD of the DES, as well as the dissolving 0.2 g of CNC in the varied ratio of the HBD of the DES, was conducted through FTIR spectroscopy to observe potential shifts in chemical bonds during the formation of DES, and for the dissolved CNC in the DES. The samples were analyzed using an attenuated total reflection FTIR spectrometer (Perkin Elmer, Frontier, USA) equipped with OMNIC software. At a resolution of 4  $\text{cm}^{-1}$ , the spectra were obtained between 4000 and 400  $\text{cm}^{-1}$  (Ramli et al., 2024).

### ii. $^1\text{H}$ NMR Analysis for the DES and CNC dissolved in DES

The nuclear magnetic resonance (NMR) study aimed to gain molecular-level insights into DES and when the CNC is dissolved in DES at varied ratios of the HBD of the DES. This was done by examining proton ( $^1\text{H}$ ) spectrum modifications. The spectra were recorded at 500 MHz using a room-temperature NMR spectrometer (Bruker et al.). Dimethyl sulfoxide (DMSO- $d_6$ ) served as the internal standard for the samples. (Ramli et al., 2022a). The

chemical shifts were calculated by DMSO-d6's retained proton resonance (2.50 ppm) (Ai et al., 2023).

iii. XRD Analysis of the Regenerated CNC

Phase identification of reinforcing fillers with CNC dissolved in different ratios of HBD of the DES was conducted using a Rigaku Mini-flex X-Ray Diffractometer (Mini-flex II, USA). As seen in **Figure 1**, the regenerated CNC at varied ratios of the HBD of the DES was exposed to X-ray radiation with a wavelength of 1.54 Å using CuK $\alpha$  radiation filtered by a Ni filter. The X-ray source operated at 30 kV and 15 mA, covering a 2 $\theta$  angle range of 10–80° throughout the analysis. To determine the Crystallinity Index (CI), Origin Pro 2018 64-bit software utilized the deconvolution method on the XRD data. The CI was calculated as the ratio of the area under each crystalline peak, identified after deconvolution, to the total area under the entire XRD curve (including non-crystalline fraction) following Equation 1 (Guimarães Junior et al., 2018). Also, the crystal size D<sub>002</sub> was determined using Equation 2, as supported by (Rocky & Thompson, 2021).

$$\text{Crystallinity Index}(\%) = \frac{\sum A_{\text{crystalline peaks}}}{\sum A_{\text{crystalline peaks}} + A_{\text{amorphous region}}} \times 100 \dots\dots\dots (1)$$

$$D_{002} = \frac{k\lambda}{B_{002} \cos \theta} \dots\dots\dots (2)$$

With a diffraction pattern on the (002) lattice plane, the D<sub>002</sub> grain diameter or crystallite size was calculated, where  $\theta$  stands for Bragg's angle or the angle of the diffracted beam. The X-ray wavelength is represented by  $\lambda$ , which is 1.79 Å for Co K $\alpha$ 1 emission. In this study, the dimensionless number k—also referred to as the Scherrer constant—is set to 1. On the (002) plane, B<sub>002</sub> is the actual peak broadening at full-width half maximum (FWHM) in radians, taking instrumental broadening into account. The value of k for polymer and cellulose materials usually falls between 0.8 and 1.0, considering several aspects such as crystal orientation, FWHM, and crystal form.

iv. Thermal Stability Analysis of Carra-CNCDES Biocomposite Films

For differential thermal analysis, a 3 mg sample was heated to 400 °C in a nitrogen environment at 10 °C per minute. The melting and crystallization temperatures were ascertained by analyzing thermogram data obtained with a differential scanning calorimeter

(DSC) (Polyma214, Germany). A thermogravimetric analyzer (STA7200, Hitachi, Japan) was then used to assess the thermal properties of the carrageenan films concerning mass loss. To evaluate the films' thermal stability and breakdown behaviour, a sample with a similar weight was heated at 10 °C/min in an airflow ranging from 30 to 700 °C (Amin, 2022).

#### V. Kinetic Analysis Carra-CNCDES Biocomposite Films

The main stage of decomposition's activation energy ( $E_a$ ) was determined using Arrhenius kinetic theory and TGA analysis. It was computed from the slope of the plot of  $\ln [\ln(1/y)]$  versus  $1000/T$ , which produced a straight line using Broido's equation as given in Eq 2.

$$\ln \left[ \ln \left( \frac{1}{y} \right) \right] = - \left( \frac{E_a}{RT} \right) + \ln A \quad \dots \dots \dots (1)$$

The conversion degree, represented by  $y$ , was determined using Equation 1, where  $A$  is the pre-exponential factor,  $T$  is the temperature measured in Kelvin (K),  $R$  is the universal gas constant ( $R= 8.314 \text{ J.mol}^{-1} . \text{K}^{-1}$ ), and  $E_a$ . Is the activation energy (kJ/mol).

$$Y = \frac{w_t - w_\infty}{w_0 - w_\infty} \quad \dots \dots \dots (2)$$

where  $w_t$  is the weight that has not yet decomposed,  $w_0$  is the original weight, and  $w_\infty$  is the residue weight (Ramli et al., 2023).

#### vii. Viscosity measurement of the Carra-CNCDES formulation

The viscosity of the reinforced carrageenan biocomposite with the CNC dissolved in varied ratios of the HBD of the DES was determined with a rotational rheometer (Rheo3000, USA) fitted with an LCT 254000010 geometry. The measurement block was filled with around 15 milliliters of the composite solution. A setup of 100 measurement points at a temperature of 40°C and a rotational speed of 300 revolutions per minute was used for the measurement (Ramli et al., 2024).

#### viii. Mechanical Properties Analysis of the Carrageenan Biocomposite Films and the Hard Capsules

The mechanical property's objective was to assess how the produced carrageenan biocomposite films and the hard capsules would deform in applied force or load. The length of the Carra-CNCDES film strips varied from 2 to 10 cm and were measured for tensile strength and elongation at break using a texture analyzer (CT3, USA) fitted with a 5 N load

cell. With a maximum displacement of 15 mm, the trigger force was applied at a crosshead speed of 30 mm/min (Hamdan et al., 2021). A loop test on hard capsules was also conducted using the same texture analyzer (CT3, USA). The test was carried out at a target of 5.0 mm and a speed of 0.50 mm/s (Sun et al., 2024). The maximal force (N) needed to rip the hard capsule before rupturing was used to calculate its loop strength.

$$\text{Tensile strength (MPa)} = \frac{\text{Load at break}}{\text{Initial width} \times \text{Initial thickness}} \dots\dots\dots (3)$$

$$\text{Elongation at break (\%)} = \frac{\text{Enlogation at rupture}}{\text{Initial guage length}} \times 100\% \dots\dots\dots (4)$$

ix. Moisture Content Analysis of the Carrageenan Hard Capsules

Their moisture content can influence the mechanical and thermal stability of hard capsules. Therefore, a moisture analyzer was utilized to determine the capsule moisture content. The initial weight of the capsules, as well as the final mass after the heating process was completed, were compared to their original mass to calculate the moisture content (Yang et al., 2020). The measurement concluded once the sample's moisture content stabilized at a constant value.

x. Disintegration Analysis of the hard capsules

A Distek 3100 disintegration tester (Germany) was used to conduct a disintegration test following USP requirements. The testing tubes containing the capsules were submerged in 600 ml of distilled water that was kept at  $37 \pm 2^\circ\text{C}$  (Silva et al., 2018). Paracetamol was employed as a placebo in the capsules to facilitate observation. The disintegration time was determined by measuring the time (minutes) required for the paracetamol to diffuse from the capsules into the medium initially.

xi. Morphological Analysis

The Carrageenan biocomposite film surface morphology was investigated using a scanning electron microscope (S26000-N, Hitachi, Japan). A platinum layer was sputter-coated onto the sample to stop the surface charge from the electron beam. The film was observed at a magnification of 1000× to assess its aggregation and surface morphology. A picture of the formed hard capsules was also observed (Thi & Lee, 2019).

## Results and Discussion

### 3.1 Functional Group Determination of Cellulose Nanocrystal (CNC) dissolved in DES

The FT-IR spectra typically reveal characteristic peaks such as the O-H stretching vibrations around  $3287.75\text{ cm}^{-1}$ , C-H stretching within  $2800\text{-}3000\text{ cm}^{-1}$ , and C-O-C stretching between  $1000\text{-}1200\text{ cm}^{-1}$ . The addition of different ratios of HBD in DES significantly impacts the FT-IR spectra during the dissolution of CNC (Nandiyanto et al., 2019). At a 1:1 ratio of the HBD of the DES, the FT-IR spectra showed slight broadening or shifting of the O-H stretching band, indicating initial hydrogen bond interactions between CNC and HBD. Still, the impact may be limited due to insufficient HBD. Peaks associated with the crystalline regions of cellulose indicating the presence of the double bonds, as the  $\text{CH}_2$  bending peak at  $1653.73\text{ cm}^{-1}$  (Hospodarova et al., 2018), were prominent, suggesting that the crystalline structure is not significantly disrupted. The C-O-C stretching region between  $1000\text{-}1200\text{ cm}^{-1}$ , as shown in **Figure 1**, indicates interaction and disruption of glycosidic linkages. At 1:2 HBD ratios, the O-H stretching band typically broadens and shifts more, reflecting increased hydrogen bonding interactions between cellulose and the HBD of the DES. It is good to note that, at the ratio of 1:2 and 1:3, the intensity of the double bond's peaks seen at  $1652.88$  and  $1652.27\text{ cm}^{-1}$  reduced, further analysis was taken to ascertain the ratio of the DES that had more impact on the cellulose dissolution process. It is seen that at 1:3 HBD ratios, the peak intensity around  $3287.75\text{ cm}^{-1}$  increased more than other ratios, this indicates hydrogen bond breakdown and interactions with cellulose and DES, It also shows the presence of the C-H bond, there is more presence of the single bonds at this ratio, indicating substantial disruption of the double and triple bonds of the cellulose crystalline regions and a transition to a predominantly amorphous structure (Liu et al., 2020). The broadening of the O-H stretching band in the FT-IR spectra with increasing HBD ratios reflects the breakdown of hydrogen bonds in cellulose (Tang et al., 2021). The observed spectral changes across different HBD ratios provide valuable insights into CNC's dissolution behaviour in the presence of DES. At a lower HBD ratio of 1:1, the limited disruption of hydrogen bonds results in reduced chemical interactions, which may lead to less effective reinforcement of the biocomposite. As the HBD ratio increases to 1:2 and 1:3, more extensive

disruption of hydrogen bonds occurs, aiding the formation of new functional groups and interactions. A 1:4 ratio of the HBD in the DES revealed the presence of double bonds without notable structural changes, indicating that the HBD ratio should be optimized, as further increases beyond the optimum may not result in significant modifications.

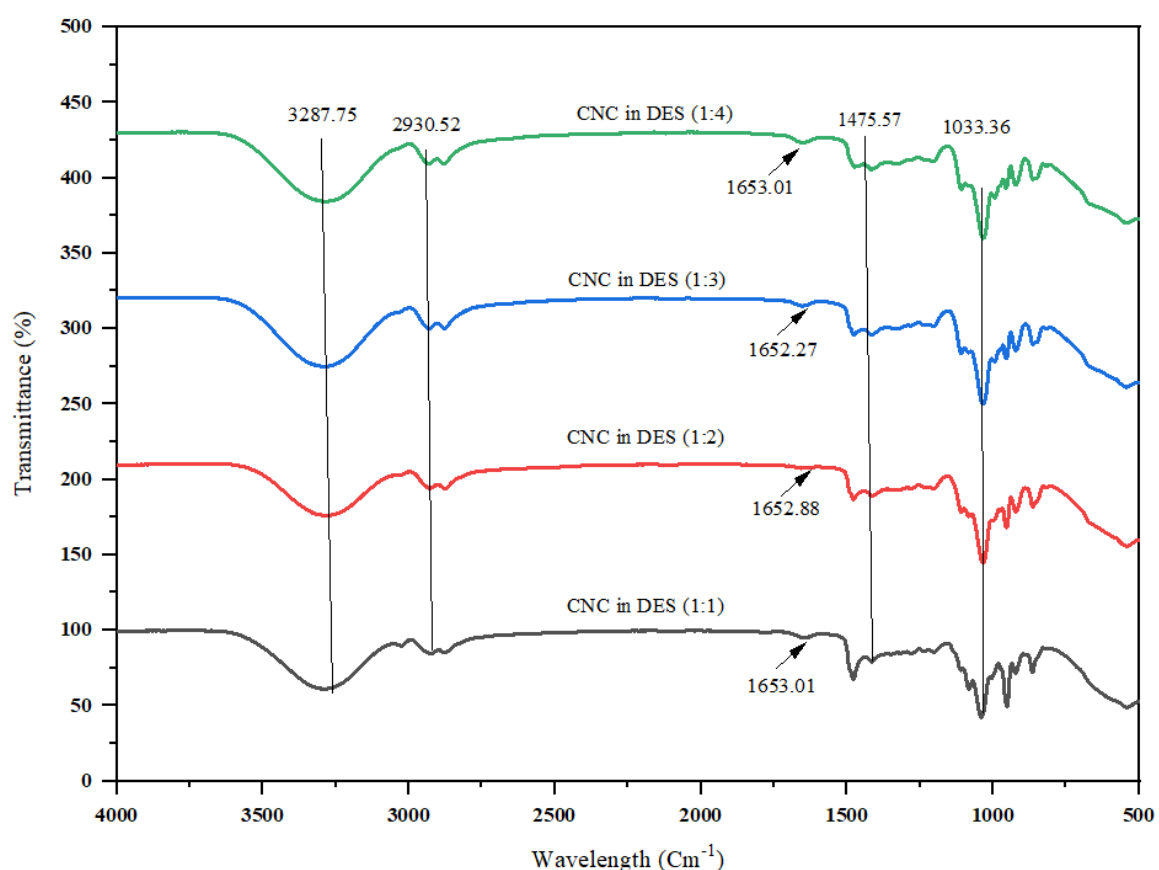


**Figure 1:** FTIR of CNC dissolved in varied ratios of the HBD of the DES

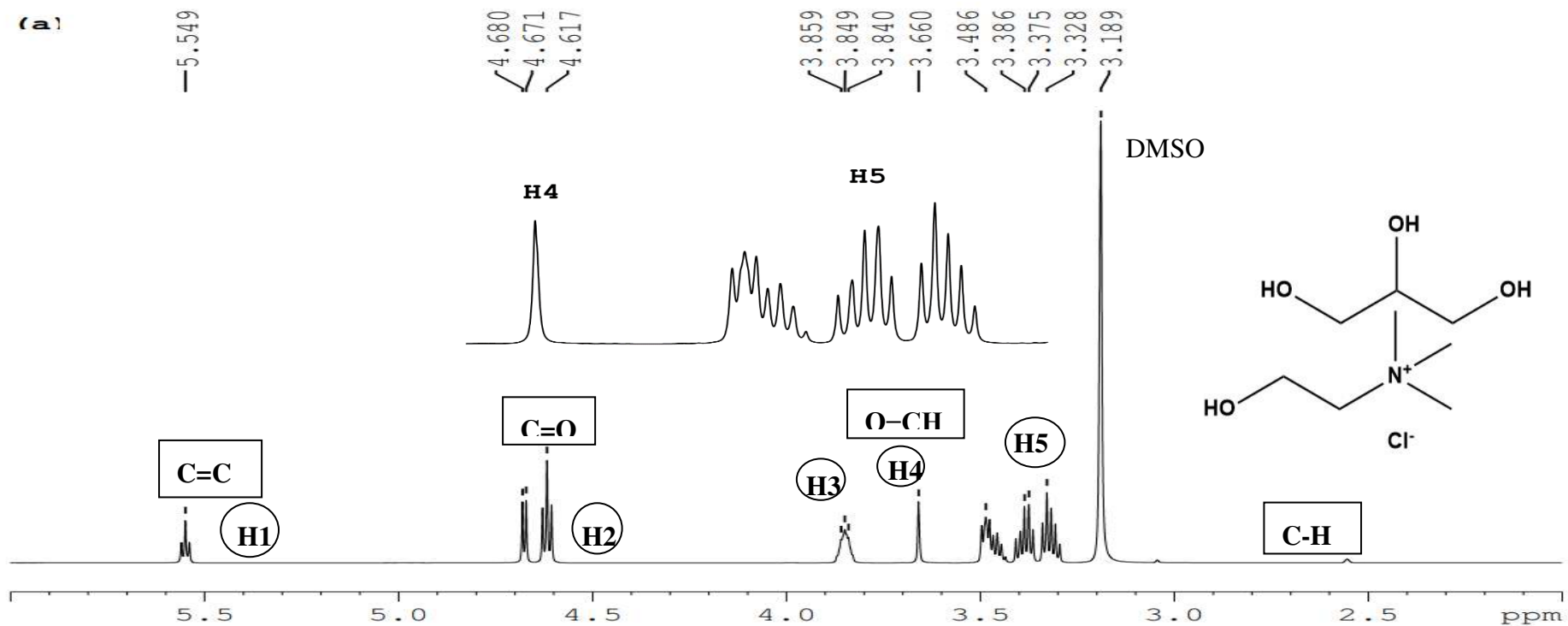
### 3.2 Effect on choline chloride glycerol-based DES on $^1\text{H}$ NMR Spectra

This study investigated the impact of varying ratios of HBD of the DES, specifically from 1:1, 1:2, 1:3, and 1:4, and their behaviour on the  $^1\text{H}$  NMR spectra in order to determine how these ratios will influence nanocellulose dissolution since the more available hydrogen bond donor present in the DES, the higher the rate of dissolution (Barani Pour et al., 2024) until a point of saturation is reached. Choline chloride ( $((\text{CH}_3)_3\text{N}(\text{Cl})\text{CH}_2\text{CH}_2\text{OH})$ ) was used as the HBA, with N, Cl, and OH as the active site of hydrogen bond acceptor and glycerol

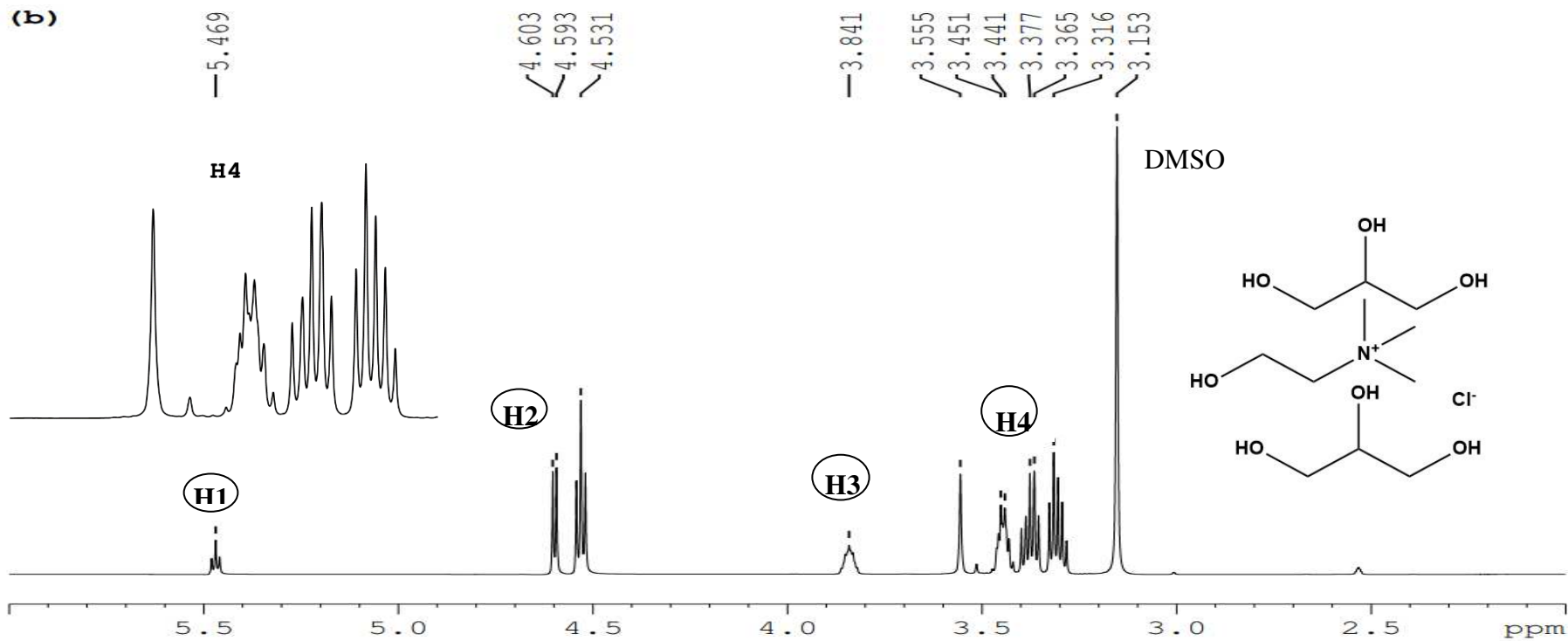
(HOCH<sub>2</sub>CH(OH)CH<sub>2</sub>OH) as the HBD with the three OH groups as the active site of hydrogen bond donation, Varied ratios of the HBD of the DES were prepared and analyzed through the <sup>1</sup>H NMR spectroscopy, with DMSO<sub>4</sub>-d<sub>6</sub> employed as a reference standard. At a 1:1 ratio, the signal ranged from 0 to 5.56 ppm, with significant integrals, as stated in **Table 1** is identified as H1 (three protons at 5.57 ppm, indicating C=C bonds), H2 (five protons at 4.65 ppm, reflecting O–C–H bonds), this is in the range that also demonstrates the presence of Glycerol as reported Bisht et al., (2021), H3, H4, H5 (thirty signals at 3.84, 3.66 and 3.23 ppm respectively indicating C=O bonds and two peaks at 1.238 and 1.207 ppm indicative of C–H bonds) as shown in **Figure 2**. The position of the integrals on the spectra at ratio 1:1 will be a reference to understand the chemical shifts that occurred on varying the HBD. As the ratio of glycerol increased to 1:2, a chemical shift occurred at H4, where the protons moved upfield due to the interaction that occurred in DES. This shows the breakdown of hydrogen bonds present as C=O to O–C–H (Speciale et al., 2022), which indicates that an increase in HBD of the DES led to the disintegration of the hydrogen bond network present in the DES (Bashir et al., 2023). An extra peak at 3.52 ppm appeared at the increase of the ratio of HBD in the DES, showing the presence of an additional proton on the spectra. Also, the peaks at 3.45 ppm disappeared, showing that a neutralization reaction occurred (Verma et al., 2024). Increasing the glycerol ratio to 1:3 resulted in more available peaks at H2 (4 protons) and H4 (93 protons) in the <sup>1</sup>H NMR spectra (Ai et al., 2023); this is also in line with the FTIR finding, which signifies that there are more HBD.

When the ratio was further increased to 1:4, peaks at H1 and H2 were reduced. In contrast, peaks at H3 and H4 increased, indicating a higher presence of C–H bonds and suggesting more available protons beyond the saturation point. This demonstrates that beyond a 1:3 ratio, additional glycerol does not significantly change the proton environment, pointing to a saturation threshold where maximum proton availability in the DES is reached. These observations highlight the necessity of precise control over the HBD-HBA ratio to optimize DES for dissolving cellulose and other biopolymers. The study's findings contribute to a deeper understanding of DES behaviour, emphasizing the importance of optimal ratios for effective DES solvent systems. Also, the knowledge is crucial for developing efficient and sustainable processes in biopolymer applications, where the solubility and interaction of components are critical for performance and functionality.

(a)



(b)



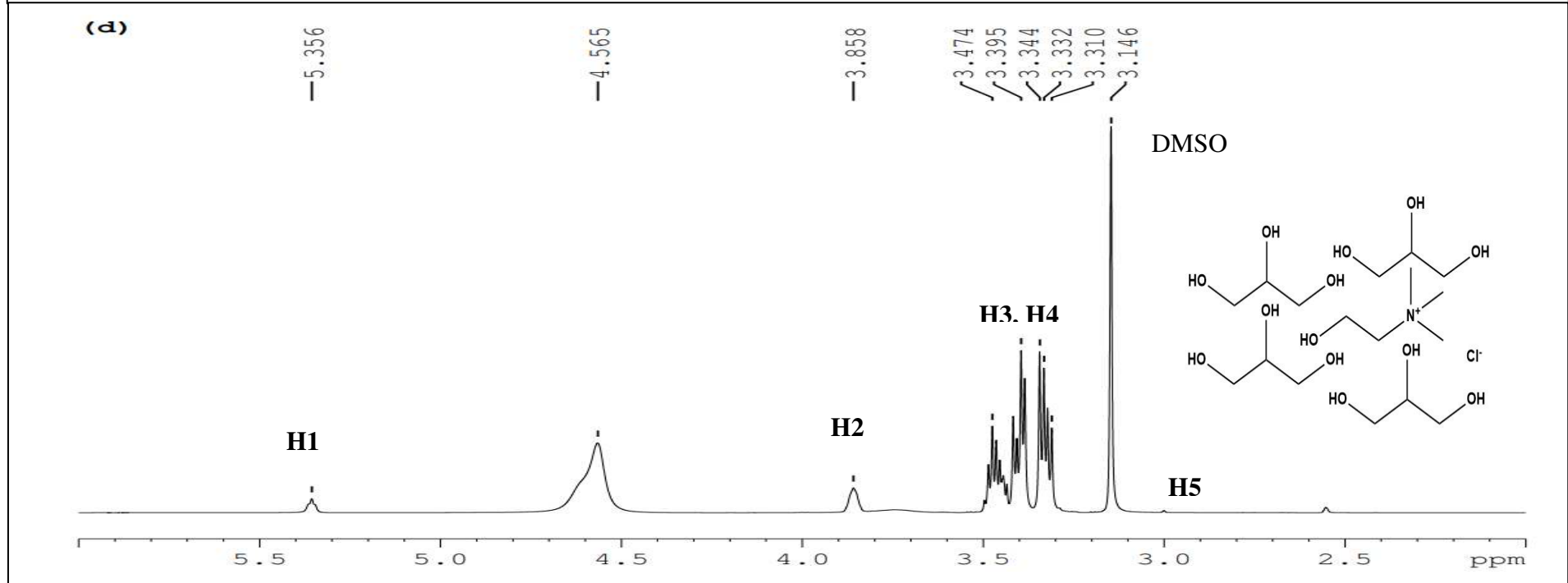
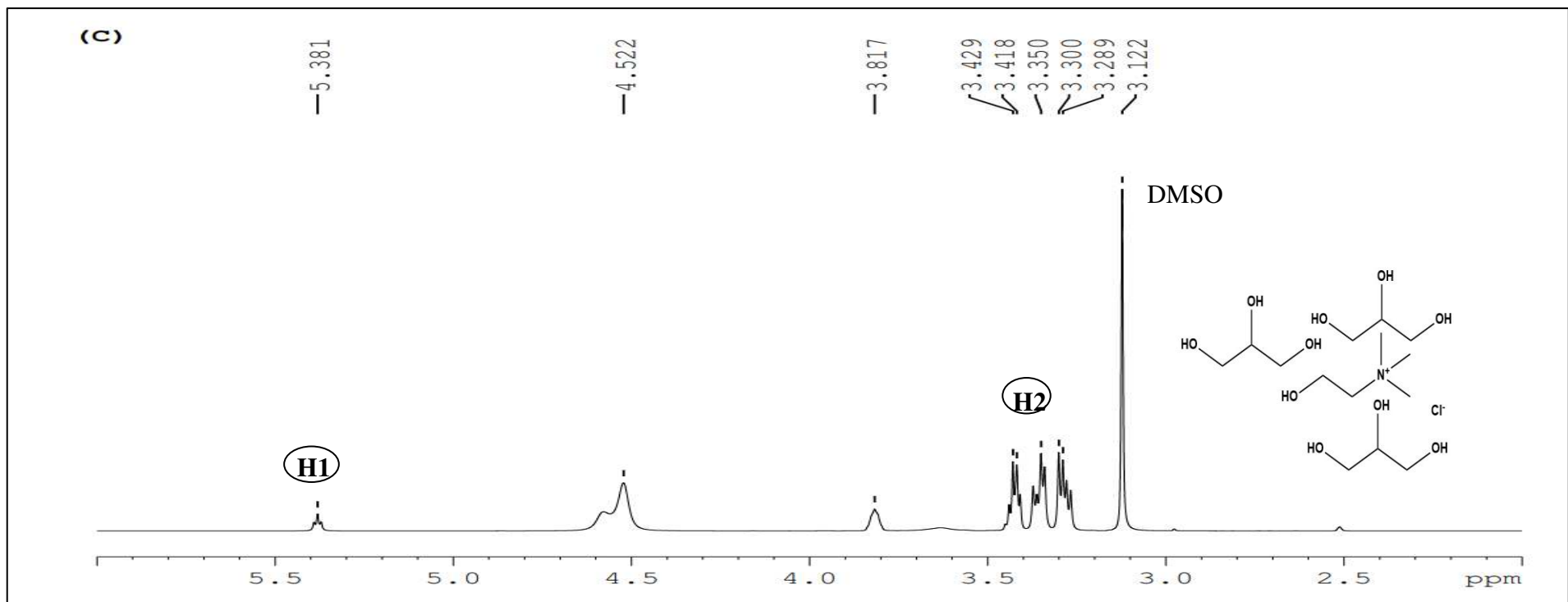


**Figure 2:** Complex  $^1\text{H}$  NMR Spectra of DES (a) ChCl Gly at the ratio of (1:1) (b) ChCl Gly at the ratio of (1:2) (c) ChCl Gly at the ratio of (1:3) (d) ChCl Gly at the ratio of (1:4)

**Table 1:**  $^1\text{H}$  NMR results by comparing their different Integrations for the varied HBD in DES

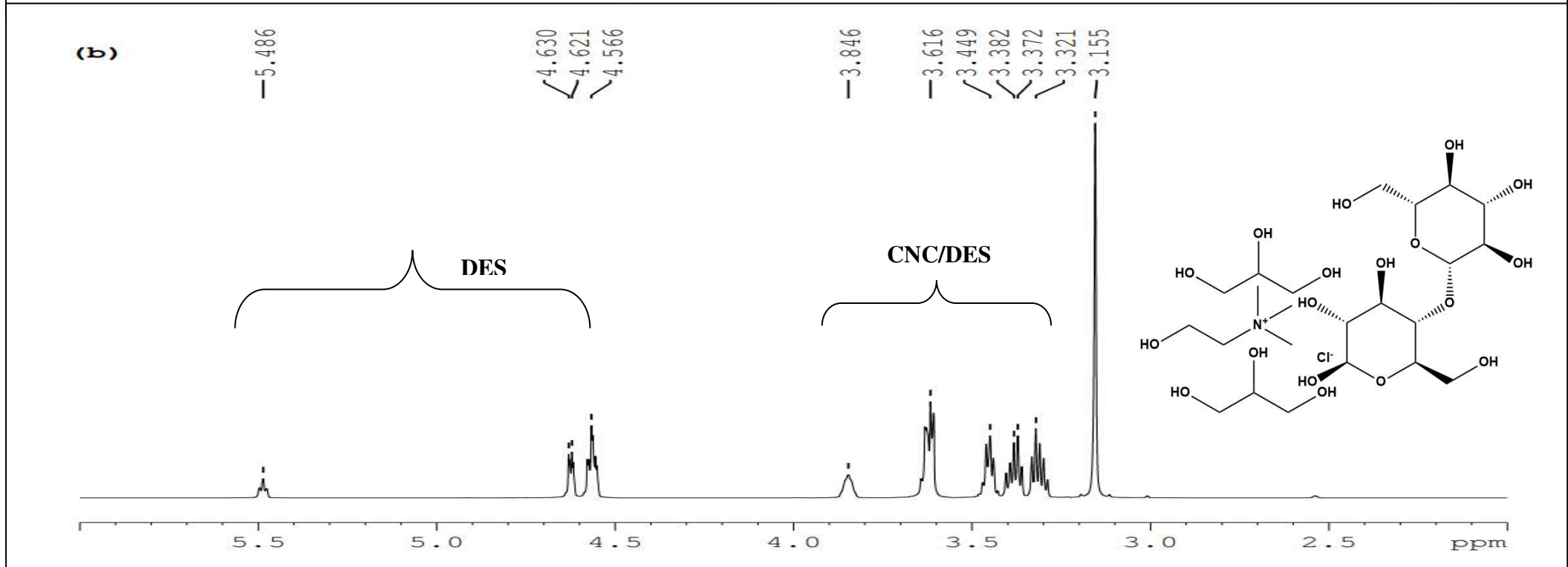
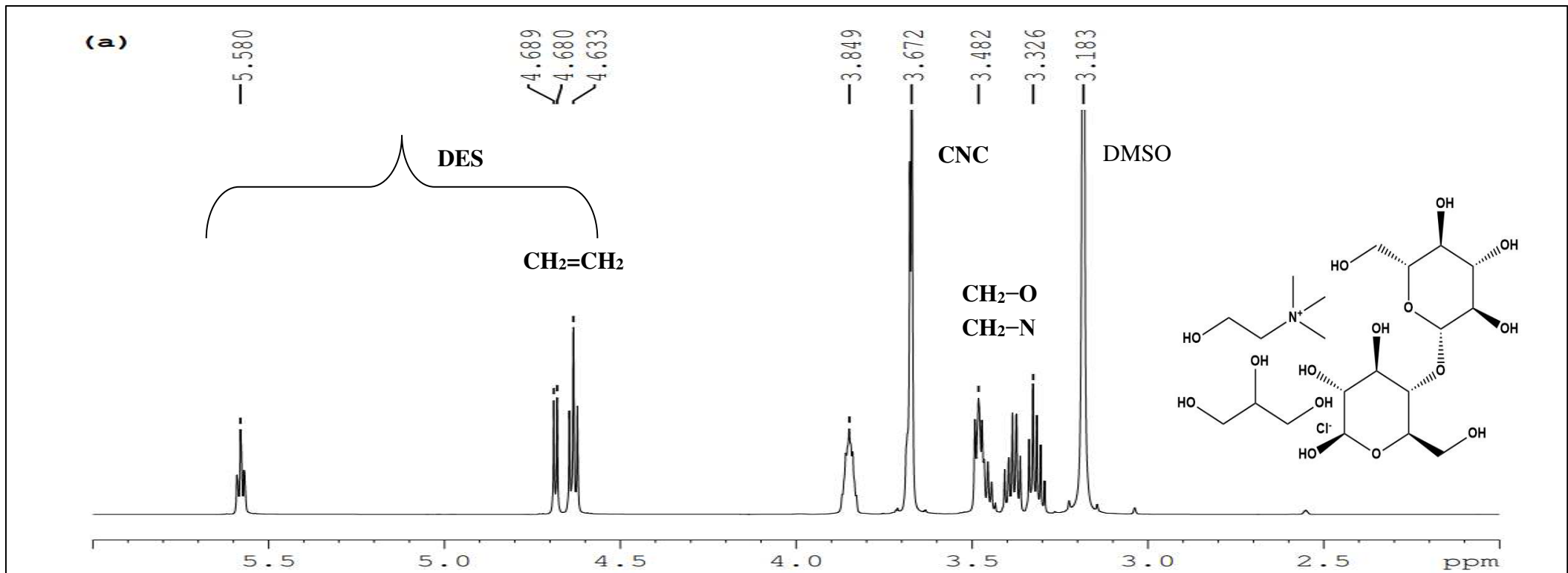
<b>Samples of Carra- CNCDES Biocomposite Films reinforced with Varied HBD</b>	<b>Integrals</b>	<b>Position on the Spectra</b>	<b>Number of Protons</b>
ChCl Gly (1:1)	H1	5.57	3
	H2	4.65	5
	H3	3.84	3
	H4	3.66	3
	H5	3.23	24
ChCl Gly (1:2)	H1	5.46	3
	H2	4.54	5
	H3	3.88	7
	H4	3.36	30

ChCl Gly (1:3)	H1	5.42	4
	H2	3.65	93
ChCl Gly (1:4)	H1	5.36	3
	H2	4.60	1
	H3	3.90	3
	H4	3.40	24
	H5	3.14	5

---

### 3.3 Effects of CNC dissolved in choline chloride glycerol-based DES on $^1\text{H}$ NMR Spectra

$^1\text{H}$  NMR spectroscopy emerges as a potent technique for unravelling the intricate solvation dynamics and molecular interactions underlying the dissolution of CNC within DES. The  $^1\text{H}$  NMR spectra, encompassing chemical shift assignments, peak intensity variations, and spectral deconvolution, gained insights into CNC's solvation behaviour and chemical environment in DES solutions (Hamdan et al., 2024). Upon dissolution of CNC in the DES, the  $^1\text{H}$  NMR results revealed 22 distinct spectral signals, indicating a substantial interaction between the DES's protons and the CNC's hydrogen bonds. This interaction was further elucidated by observing three distinct ranges in the spectra. The first range, H1, as seen in **Figure 3**, spanning from 1.31 to 1.51 ppm, corresponds to the aliphatic group (C-H), while the subsequent range, H2 to H4, observed between 3.24 and 3.95 ppm, signifies the presence of (C-H-O) functionalities. The final range, H5 to H7, detected at 4.17 to 6.30 ppm, indicates the anomeric group (Penner & Vulpetti, 2024). Notably, there was a shift of highly double bonds in the spectra. This aligns with the earlier experimental hypothesis, suggesting the breakdown of hydrogen bonds within cellulose, ultimately leading to its dissolution. This finding underscores the pivotal role of DES in facilitating the disruption of cellulose bonds and highlights its potential as a solvent for cellulose dissolution processes. The distinctive chemical shifts observed in the spectra at 0.02 ppm, 6.17 ppm, and 3.84 ppm indicate the presence of the C-Cl, N-H, and C-O bonds, respectively. This elucidates the solute-solvent interactions of HBD and HBA and sheds light on the extent of CNC dissolution and the influence of DES composition on CNC solubility (Cao et al., 2016). Moreover, quantitative analysis enables accurate determination of CNC concentration and dissolution efficiency, facilitating precise control over CNC dispersion and utilization in various applications. By correlating spectral features with solvent properties and CNC characteristics,  $^1\text{H}$  NMR analysis unveils the underlying solvation mechanisms governing CNC dissolution, paving the way for the rational design of CNC-based materials with tailored properties and enhanced performance. Understanding CNC solvation dynamics in DES increases fundamental knowledge of cellulose dissolution processes. This holds significant implications for developing sustainable and eco-friendly nanocellulose-based materials for various industrial applications.



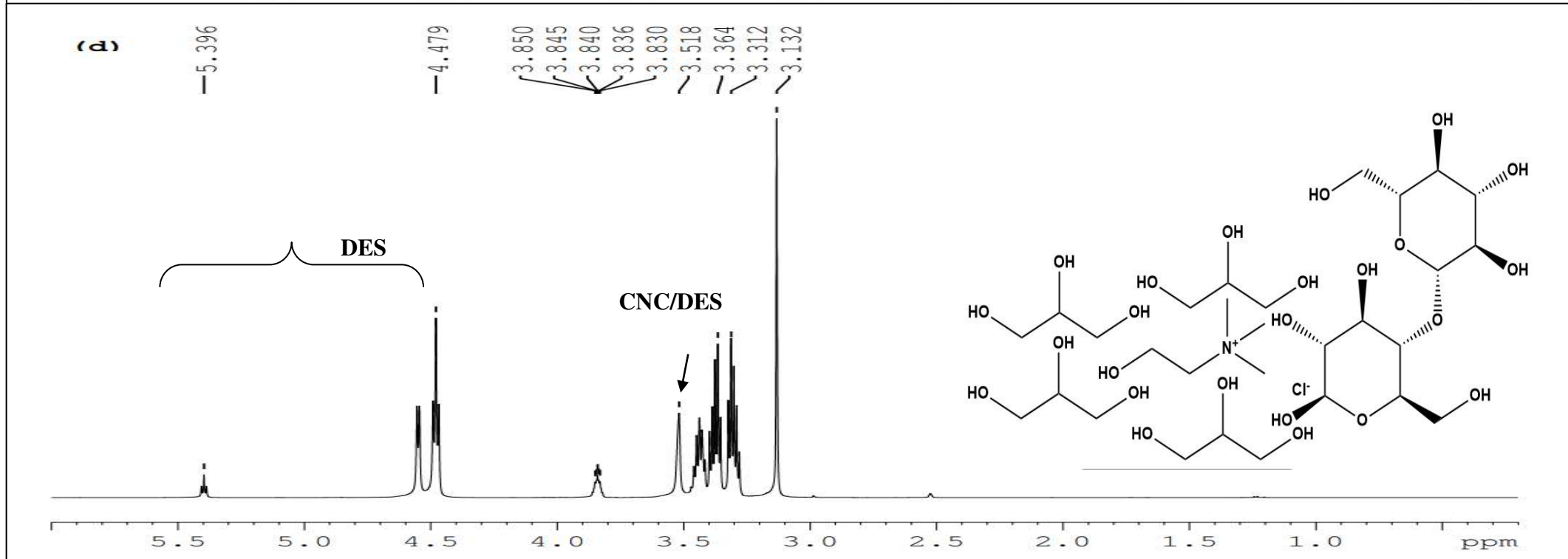
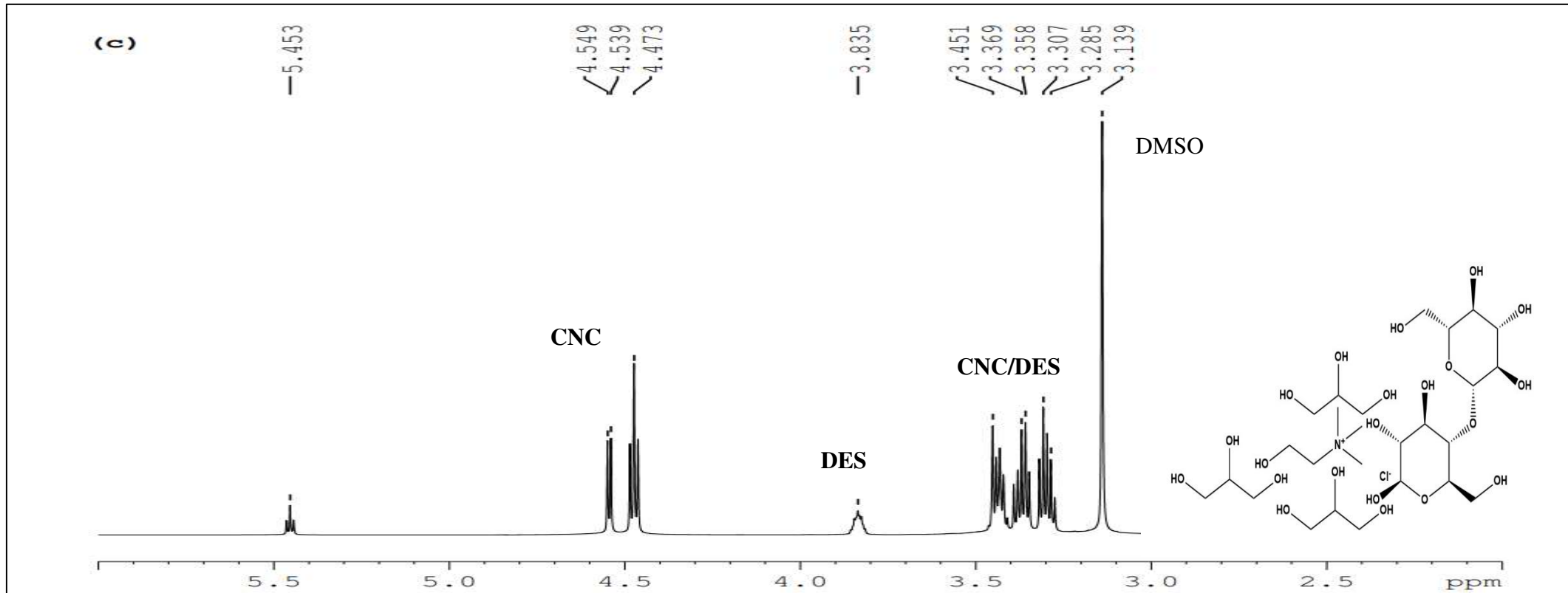


**Figure 3:** Complex  $^1\text{H}$  NMR Spectra of CNC dissolved in DES (a) CNC in ChCl Gly at the ratio of (1:1) (b) CNC in ChCl Gly at the ratio of (1:2) (c) CNC in ChCl Gly at the ratio of (1:3) (d) CNC in ChCl Gly at the ratio of (1:4).

### 3.4 XRD Analysis of Carra-CNCDES Film in Varied Ratios of HBD

The X-ray diffractogram in Figure 4.9 demonstrates a relatively ordered structure in the CNC sample, characterized by a sharp, narrow peak at  $2\theta = 22.3^\circ$  as seen in **Figure 5**, corresponding to the (200) plane, and a broader peak spanning  $14.5^\circ$  to  $16.2^\circ$ , which represents the overlapping (010) and (110) planes of cellulose I. The distinct peak at  $2\theta = 22.3^\circ$ , as shown in **Table 2**, indicates it is the primary diffraction peak of cellulose, reflecting the ordered crystalline nature of the CNC (Ramírez-Wong et al., 2016). Additionally, the diffraction peak at  $2\theta = 34.6^\circ$  is associated with the (004) lattice plane of cellulose I (Pang et al., 2023).

The single broad peak, formed by the overlapping of (010) and (110) planes, suggests a decrease in crystallinity due to dissolution, as indicated by the large full width at half maximum (FWHM) of these peaks Tamaddon et al. (2023). This broadening effect points to the impact of dissolution on the CNC, with crystalline regions disrupted and crystal size potentially reduced, aligning with the CI reduction (Guimarães Junior et al., 2018; Shoaib et al., 2023). In this study, the crystallinity index (CI) values obtained at varied ratios of HBD show a significant decrease, attributed to the reduction in crystalline regions, indicating increased disorder within the crystal lattice and a reduced crystalline phase (Gundupalli et al., 2023). The minor peak observed at  $2\theta = 34.6^\circ$  for the (004) plane became less pronounced following hydrolysis but was more defined post-dissolution. These observations suggest that the regenerated CNC retains a cellulose I structure, indicated by the absence of a doublet and a peak characteristic of cellulose II (Bangar et al., 2022). The  $^1\text{H}$  NMR findings also support this. However, the calculated CI may be lower than the actual value due to the minimal peaks identified in the crystal structure fitting (Smith et al., 2020). Additionally, the non-accounted peak overlaps may have influenced FWHM values, affecting the minimum intensity related to the amorphous regions, which might suggest enhanced dissolution effects in the cellulose structure.

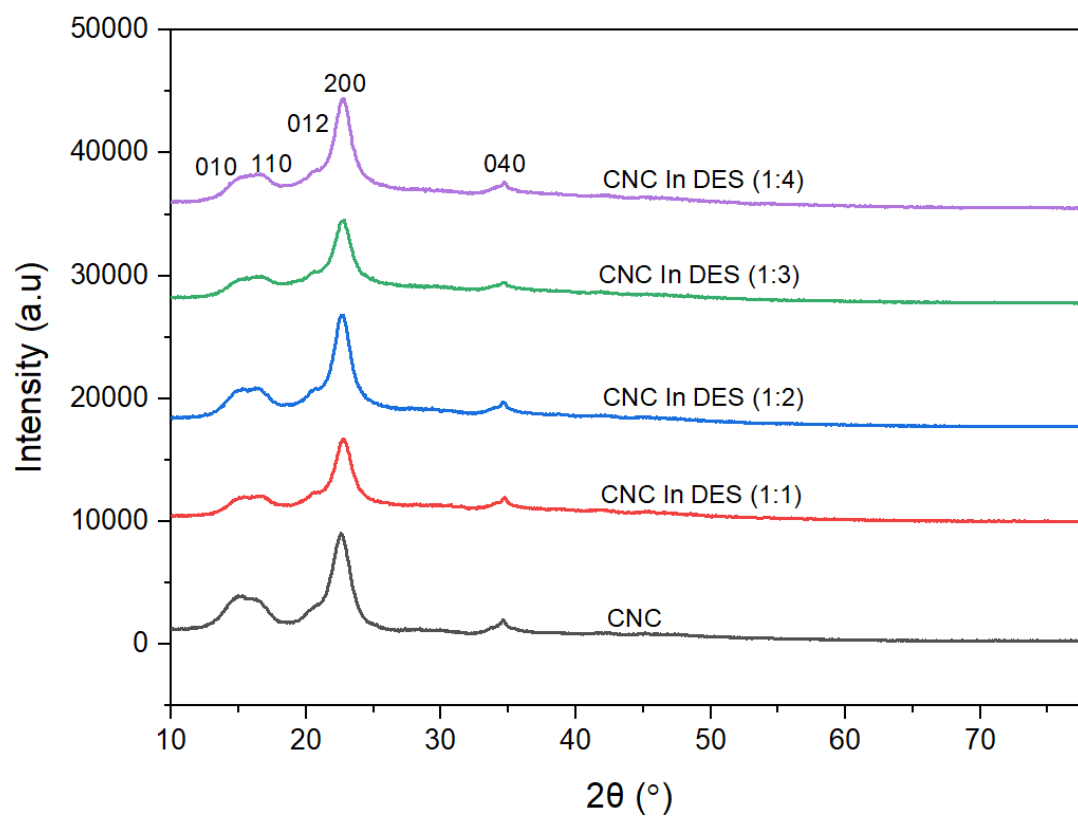


**Figure 4:** XRD of CNC and CNC dissolved in DES

**Table 2:** Size of crystallites, reflection planes, diffraction angles, interplanar distances, and the crystallinity Index

<b>Samples of CNC, CNC dissolved in Varied HBD</b>	<b>Lattice Plane (hkl)</b>	<b>Diffraction angle, 2<math>\theta</math> (<math>^{\circ}</math>)</b>	<b>Interplanar Spacing (<math>\text{\AA}</math>)</b>	<b>Crystallite dimension (<math>\text{\AA}</math>)</b>	<b>Crystallinity Index (%)</b>	<b>Crystal Size (nm)</b>
CNC	010	14.54	6.09	37	74	1.67
	110	16.00	5.53	24		
	012	22.20	4.00	27		
	200	22.64	3.92	75		
	040	34.59	2.59	87		
CNC In DES (1:1)	010	14.83	5.97	77	27	1.72
	110	16.26	5.44	49		
	012	22.44	3.96	26		
	200	22.79	3.90	71		
	040	34.67	2.58	78		
CNC In DES (1:2)	001	14.83	5.97	55	34	1.29
	010	16.43	5.39	49		
	110	21.07	4.21	38		
	012	22.52	3.94	73		

	200	22.95	3.87	43		
	040	34.61	2.59	92		
CNC In DES (1:3)	010	15.92	5.56	37	38	1.26
	200	22.66	3.92	41		
	040	34.63	2.59	101		
CNC In DES (1:4)	010	15.88	5.58	34	35	1.34
	200	22.67	3.92	41		
	040	34.67	2.59	80		

---

### 3.5 Thermal Analysis and Broido's Kinetic Model of Carra-CNCDES Film in Varied Ratios of HBD.

A detailed analysis of the thermal properties of the Carra-CNCDES films was conducted to ascertain their potential applicability in the pharmaceutical industry, particularly for use in hard capsules. This study delved into the thermal behaviour of these films by employing advanced techniques such as DSC, TGA, and Broido's kinetic model. This focuses on dissolving CNC in a DES with varying ratios of HBD to HBA, aiming to optimize the thermal properties and stability of the resultant carrageenan biocomposite films. Initial solubility studies revealed that a 1:3 ratio of HBD to CNC offered optimal solubility, which served as a benchmark for further thermal stability analysis. TGA thermograms identified distinct thermal degradation stages at various HBD ratios, providing critical insights into the composite films' decomposition behaviour (Tamaddon et al., 2023). At a 1:1 ratio, the thermograms revealed four stages: the first stage at 45.6 °C involved the degradation of volatile components such as moisture, indicated by a weight loss of 11.35%, suggesting that the films begin to melt and free water is removed when heated from ambient temperature to 100°C, this was supported by (Ramli et al., 2022). The second stage, observed at 228.4 °C, marked the volatilization of plasticizers within the film matrix. In contrast, the third stage at 292.2 °C corresponded to the decomposition of the Carra-CNCDES polymer chain and cross-linkers, as reported by Adam et al. (2020). The fourth stage, occurring at 442.8 °C, was identified as the recrystallization temperature. Increasing the HBD ratio to 1:2 introduced a fifth weight loss stage at 115.12 °C, attributed to the evaporation of loosely bound moisture, while further increases to 1:3 and 1:4 ratios added additional weight loss stages, likely due to the evaporation of more volatile liquids, possibly by-products of the interaction between carrageenan, CNC, and DES. Derivative DTG curves plotted to identify peak temperatures for maximum weight loss during thermal decomposition indicated that for the CNC Gly (1:1) film, the peak temperature was 242 °C, as shown in **Figure 5**. Increasing the HBD ratio to 1:2 elevated this temperature to 244 °C. At a ratio of 1:3, 245 °C was recorded and seen in **Table 3**, slightly higher than other ratios. At the same time, at 1:4, the temperature dropped to 239 °C, collaborating with initial reports from <sup>1</sup>H NMR and XRD that the 1:3 ratio yields optimal results with 0.2 g of CNC dissolved in 10 g of DES. However, at a 1:4 ratio, the peak temperature decreased, suggesting that the saturation point of DES had been reached, and further increases in HBD do not significantly affect the carrageenan film and hard capsules' thermal behaviour. Kinetic analysis used Broido's mathematical model to further analyze

these films' thermal stability. Broido's model, which allows the calculation of activation energy ( $E_a$ ) from a single TGA curve, unlike other models that require multiple analyses with different heating rates, revealed that the major decomposition for all films occurred between 200 and 400 °C. The  $E_a$  values calculated from this range showed high determination coefficients ( $R^2 > 0.83143$ ), indicating a good fit to Broido's model. At a 1:3 ratio, the film exhibited an  $E_a$  of 76.77 kJ/mol, as seen in **Table 4**, reflecting the highest resistance to molecular structure degradation due to temperature. This increased  $E_a$  is linked to the dissolution of CNC within the carrageenan matrix, enhancing heat distribution and delaying film decomposition. It also presented a good fit for depicting thermal degradation when applying Broido's model since high values of the determination coefficient were achieved ( $R^2 > 0.8$ ), as shown in **Figure 5d**. The study also evaluated the enthalpy changes ( $\Delta H$ ), entropy ( $\Delta S$ ), and Gibbs energy ( $\Delta G$ ) during the thermal degradation process to provide a comprehensive understanding of the thermal behaviour of these composite films. The enthalpy change ( $\Delta H$ ) reflects the energy absorbed or released during heating, where higher values indicate lower reactivity and lower values denote higher reactivity. All films reported negative  $\Delta H$  values, indicating an exothermic reaction. The entropy change ( $\Delta S$ ) values, which show the degree of disorder during bond dissociations, were negative across all films, suggesting an ordered structure and a system close to thermodynamic equilibrium, indicating low reactivity. The Gibbs energy ( $\Delta G$ ) values revealed the system's stability, with positive values indicating the non-spontaneous nature of thermal degradation (endergonic process), thus enhancing film stability. Comparative analysis of the thermal properties of different films demonstrated that at a 1:3 ratio, the residual weight of the film was 8.07  $\mu\text{g}$ , higher than other films, indicating optimal thermal properties. This finding aligns with the reinforcement studies of carrageenan films (Sedayu et al., 2020), demonstrating the positive impact of CNC dissolution in DES at this ratio. The analysis of the thermal properties of Carra-CNCDES films highlights CNC and DES's significant impact on enhancing carrageenan-based composite materials' thermal stability. The study employed advanced thermal analysis techniques such as DSC and TGA, alongside kinetic modelling using Broido's method, to elucidate the thermal behaviour of these materials. The findings of this study include the optimal CNC solubility in DES at a 1:3 ratio, which significantly enhances thermal stability and resistance to decomposition, as supported by NMR and XRD studies. This ratio also provided the highest performance in activation energy, enthalpy, entropy, and Gibbs energy changes, indicating superior thermal properties compared to other ratios. These results underscore the potential of CNCDES composites in various industrial applications,

particularly in the pharmaceutical sector, where thermal stability is crucial for developing hard capsules.

**Table 3:** Thermal degradation behaviour of films by thermogravimetric analysis

<b>Samples of Carra- CNCDES Biocomposite Films reinforced with Varied HBD</b>	<b>Step</b>	<b>Temperature range (°C)</b>	<b>Weight loss at step end (%)</b>	<b>Temperature maximum degradation (°C)</b>	<b>at Residues at 700 °C rate (%)</b>
ChCl Gly (1:1)	2	30-200	11.35	228.41	7.50
		200-700	29.10		
ChCl Gly (1:2)	2	30-200	23.58	244.34	7.87
		200-700	19.12		
ChCl Gly (1:3)	2	30-200	20.83	245.00	8.07
		200-700	17.73		
ChCl Gly (1:4)	2	30-200	22.80	238.96	8.04
		200-700	19.71		

**Table 4:** Kinetic and thermodynamic analysis of thermal degradation by Broido's model

Samples	Ea (kJ/mol)	A	R <sup>2</sup>	ΔS (J/K mol)	ΔH(kJ/mol)	ΔG (kJ/mol)
<b>Carra-CNCDES</b>						
<b>Biocomposite</b>						
<b>Films reinforced</b>						
<b>with Varied HBD</b>						
ChCl Gly (1:1)	75.10	3.96×10 <sup>-2</sup>	0.84255	-117.07	-1891.56	2.48 ×10 <sup>4</sup>
ChCl Gly (1:2)	75.05	3.97×10 <sup>-3</sup>	0.84154	-125.61	-2030.76	2.87 ×10 <sup>4</sup>
ChCl Gly (1:3)	76.77	4.04×10 <sup>-3</sup>	0.83383	-125.55	-2036.24	2.87 ×10 <sup>4</sup>
ChCl Gly (1:4)	79.64	4.19×10 <sup>-3</sup>	0.85539	-125.33	-1985.99	2.80 ×10 <sup>4</sup>

Abbreviations: ΔG: Gibbs free energy; ΔH: enthalpy; A: pre-exponential factor; R<sup>2</sup>: coefficient of determination; ΔS: entropy; Ea: activation energy.

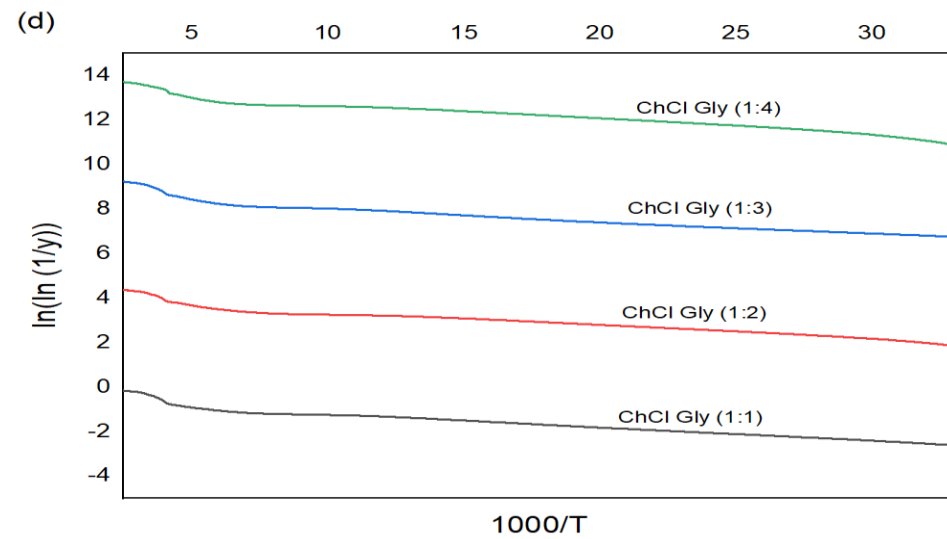
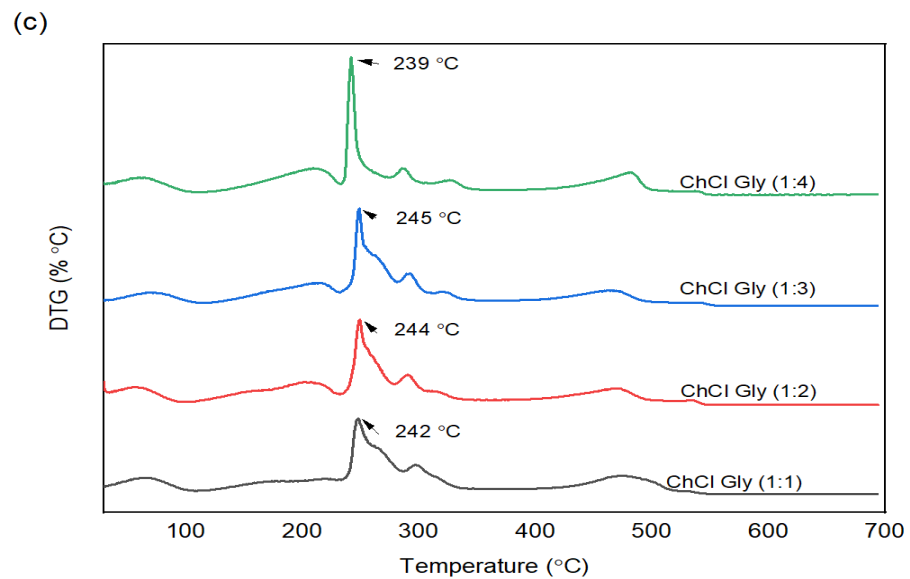
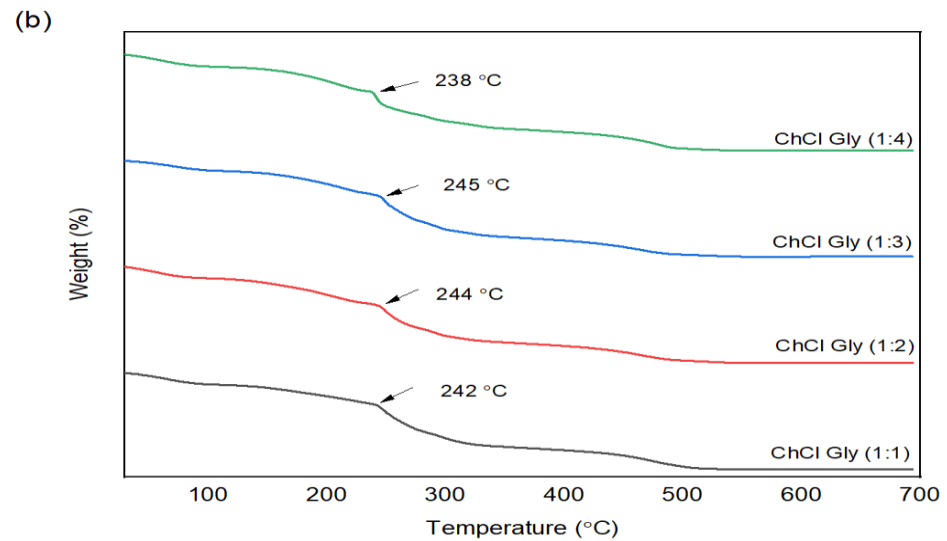
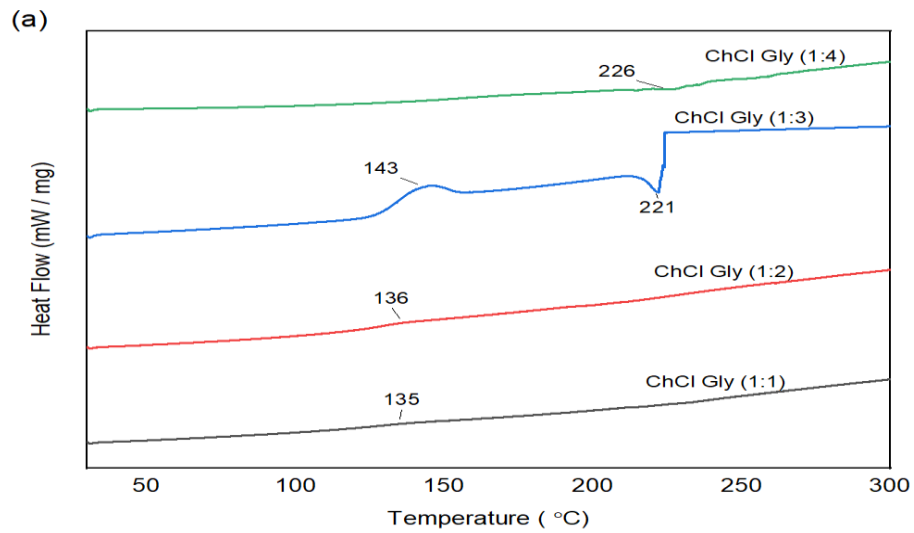


**Figure 5:** (a) Differential scanning calorimeter (DSC) thermograms of Carra-CNCDES reinforced with Varied HBD ratios. (b) TGA of Carra-CNCDES biocomposite Films, reinforced with CNC dissolved in varied HBD of DES (c) DTG thermograms of Carra-CNCDES biocomposite Films, reinforced with CNC dissolved in varied HBD of DES (d) Broido's Plot for degradation of varied HBD ratios.

### **3.6 Viscosity and mechanical properties of Carra-CNCDES biocomposite films and hard capsule**

The study of biocomposites reinforced with CNC dissolved in DES has revealed significant modifications in their mechanical properties as the ratio of HBD is varied (Manafpour et al., 2024). Specifically, adjusting the HBD ratios in DES influences the viscosity of the resulting solutions, which in turn impacts the mechanical strength of the biocomposites. In this work, it was observed that the viscosity of the CNC-DES solutions reached its peak at a 1:3 ratio of HBD to CNC. This increased viscosity at the 1:3 ratio is directly correlated with enhanced mechanical properties of the biocomposites, as evidenced by the measurements of capsule loop strength and tensile strength (Gygli et al., 2020). The data presented in **Table 5** illustrates that the highest viscosity corresponds with the greatest tensile strength and capsule loop strength values. Notably, at the 1:3 HBD ratio, the biocomposite recorded a capsule loop strength of 75.83 MPa and a tensile strength of 102.04 MPa, respectively. These findings suggest that the mechanical reinforcement of biocomposites is influenced by the viscosity of the CNC-DES solution, which is modulated by the HBD ratio (Calvo-Flores et al., 2021). The increased viscosity at higher HBD ratios likely enhances the interfacial bonding between the CNC and the polymer matrix, improving stress transfer and overall mechanical performance (Hamdan et al., 2019)). This is critical for applications where high mechanical strength and durability are required, such as in packaging materials, biomedical devices, and structural components.

The interaction networking within the CNC-DES system can be attributed to the enhanced hydrogen bonding interactions at higher HBD ratios, which result in a more viscous medium. This medium facilitates better dispersion of CNCs and more robust interactions with the polymer chains, thereby reinforcing the biocomposite structure. Additionally, the rheological

properties of the CNC-DES solutions, which are influenced by the HBD ratio, play a crucial role in the processing and fabrication of these biocomposites. Higher viscosity solutions can lead to more uniform and stable biocomposite materials (Abbasi et al., 2023), reducing defects and improving the overall quality of the final product. Therefore, understanding the relationship between HBD ratio, viscosity, and mechanical properties is essential for optimizing the performance of CNC-reinforced biocomposites. Further investigations could explore the effects of different types of HBDs and their concentrations and the interaction mechanisms at the molecular level to develop a comprehensive understanding of how these variables influence the mechanical properties of biocomposites (Amin et al., 2015). Such insights could develop tailored biocomposite materials with specific properties for targeted applications. The study also highlights the importance of balancing viscosity for practical processing considerations. While high viscosity can enhance mechanical properties, it may also challenge material handling and processing efficiency. Therefore, finding an optimal HBD ratio that maximizes mechanical strength without compromising processability is critical to successfully applying CNC-DES biocomposites in various industries (Mariano et al., 2014). The ratio of HBD in DES significantly affects the viscosity of CNC-DES solutions and, consequently, the mechanical properties of the reinforced biocomposites. The highest mechanical strength was observed at a 1:3 HBD ratio, demonstrating the critical role of viscosity in enhancing tensile strength and capsule loop strength. This correlation underscores the potential of manipulating DES compositions to tailor the properties of biocomposites for specific applications, paving the way for advanced materials with superior performance characteristics.

**Table 5:** Viscosity, Capsule Loop strength, Elongation at break, Tensile Strength, Melting Temperature (Tm) of Carra-CNCDES biocomposites and Hard Capsules reinforced with varied HBD

<b>Hard Capsules</b>		<b>Viscosity (mPa.s)</b>		<b>Loop Strength (MPa)</b>	<b>Elongation at break (%)</b>	<b>Tensile Strength (MPa)</b>	<b>Tm (°C)</b>
ChCl (1:1)	Gly	924.00 4.24	±	53.95 ± 0.80	23.51	83.35	245.89
ChCl (1:2)	Gly	1034.0 5.66	±	69.85 ± 0.71	28.38	90.84	155.12
ChCl (1:3)	Gly	1218.5 2.12	±	75.83 ± 0.57	31.90	102.04	166.86
ChCl (1:4)	Gly	1115.0 7.07	±	73.22 ± 1.06	29.69	89.68	166.81

### 3.7 Moisture content and disintegration time of the hard capsule

At a 1:1 ratio of HBD, the biocomposite film exhibited the highest moisture content at 20.19% (Table 6). This elevated moisture content can be attributed to the insufficient capacity of the HBD to effectively break down the hydrogen bonds present in the CNC and carrageenan matrix. Consequently, the sulfate groups within carrageenan, known for their high hydrophilicity, remain unaltered and contribute to the film's increased ability to absorb water (Yang et al., 2020). As the concentration of HBD increased, there was a noticeable decline in the film's affinity to adsorb water, reaching a 1:3 HBD ratio, which recorded the lowest moisture content. Beyond this ratio, further increases in HBD concentration did not result in significant reductions in moisture content. The mechanism behind this trend can be understood through the interaction dynamics between CNC, carrageenan, and HBD. At lower HBD concentrations, the DES system lacks hydrogen donors to disrupt the extensive

hydrogen bonding network between the hydroxyl groups of CNC and the sulfate groups of carrageenan (Yang et al., 2024). This results in a structure that retains a higher amount of moisture. As the HBD concentration increases, the DES system becomes more effective in breaking these hydrogen bonds, reducing the availability of sites for water adsorption and decreasing the moisture content. At the optimal 1:3 ratio, the hydrogen bonds are sufficiently disrupted, leading to a more hydrophobic network that minimizes water uptake.

This reduction in moisture content at higher HBD concentrations significantly impacts the film's mechanical properties. Lower water absorption enhances the film's tensile strength and reduces its brittleness (Thakur et al., 2019). This is due to the decrease in the plasticizing effect that water molecules impart on the polymer matrix, leading to a more rigid and robust structure. The 1:3 HBD ratio film, with a moisture content of 15.02%, demonstrated the best mechanical strength among the tested ratios, as supported by (Aiman Hamdan et al., 2021). This value is particularly notable as it is comparable to that of commercial gelatine capsules, which have a moisture content of approximately 13%, and significantly higher than that of commercial HPMC (hydroxypropyl methylcellulose) capsules, which have a moisture content of about 4.5%.

The low moisture content of the 1:3 ratio of Carra-CNCDES film also positively influences its disintegration time. Moisture content is critical in determining biocomposite films' disintegration properties in hard capsules. A lower moisture content generally correlates with slower disintegration times due to reduced water interaction and penetration within the film matrix. In this study, the 1:3 ratio film disintegrated in 7 minutes and 17 seconds, as seen in **Table 6**, aligning with the findings of (Ramli et al., 2024), who observed similar disintegration characteristics in optimized biocomposite formulations. This disintegration time is suitable for oral drug delivery applications, where a balance between mechanical strength and timely disintegration is crucial.

The findings suggest that the 1:3 HBD ratio in Carra-CNCDES biocomposite films provides a balanced optimization of mechanical properties and functional performance. The decreased moisture content enhances the tensile strength, reduces brittleness, and ensures a disintegration time within acceptable limits for pharmaceutical applications. This balance is vital for developing biocomposite films that can be effective and sustainable alternatives to traditional gelatine capsules. Moreover, the environmental and economic benefits of using plant-based materials such as carrageenan and CNC in combination with DES systems further bolster the commercial viability of these biocomposite films. The ability to tailor the properties of these films through varying HBD ratios allows for customization according to

specific application requirements. For instance, films requiring higher mechanical strength and lower disintegration times can be optimized with the 1:3 HBD ratio. At the same time, other formulations might benefit from different ratios depending on the desired end-use.

**Table 6:** Effect of Varied HBD concentration on the moisture content of film and disintegration time of hard capsule

<b>Samples of Carra-CNCDES Biocomposite Films reinforced with Varied HBD</b>	<b>Moisture Content (%)</b>	<b>Disintegration Time (min)</b>
ChCl Gly (1:1)	20.19 ± 1.64	8.50 ± 0.50
ChCl Gly (1:2)	19.85 ± 1.39	8.00 ± 0.50
ChCl Gly (1:3)	15.02 ± 1.20	7.17 ± 0.29
ChCl Gly (1:4)	19.25 ± 1.43	8.50 ± 0.50

### **3.8 Physical appearance and surface morphology of Carra-CNCDES biocomposite film.**

The biocomposite film and hard capsule transparency and gloss are well-retained until the addition of the 1:3 ratio of the HBD **Figure 6**. At this point, the film became more transparent, showing a good mixing of the CNC in DES within the carrageenan matrix. The film maintained a clear and shiny appearance, which also indicates minimal scattering and light absorption, which suggests a uniform distribution of the components (Shoaib et al., 2023). This visual clarity is crucial for applications where aesthetic and optical properties are essential, such as in packaging and pharmaceutical capsules. The uniform matrix observed in these films highlights the materials' compatibility, attributed to the practical and uniform mixing process. This homogeneity directly results from good miscibility between the biopolymers carrageenan, HPMC, and CNC within the DES system. The DES likely facilitates better interactions and hydrogen bonding among these polymers, leading to a consistent and stable composite structure (Barros et al., 2014). This is also evident from the picture of the carrageenan hard capsules, as seen in **Figure 7**.

SEM images confirm this observation by revealing smooth and continuous surface morphology without significant phase separation or aggregation (Koch & Włodarczyk-Biegun, 2020). The absence of large voids or cracks in the SEM images indicates that the components are well-integrated at the microscopic level. Additionally, the cross-sectional

views of the films show a dense and cohesive structure, supporting the notion of strong intermolecular interactions facilitated by the DES (Donato et al., 2023). As the HBD ratio is increased beyond 1:3, a slight reduction in transparency and gloss is noticed. This change could be attributed to the onset of phase separation or the formation of microdomains within the matrix, which scatter light more effectively, thereby reducing clarity. Nevertheless, the overall structure remains relatively uniform, suggesting that the films possess good mechanical properties and stability (Ramli et al., 2023).

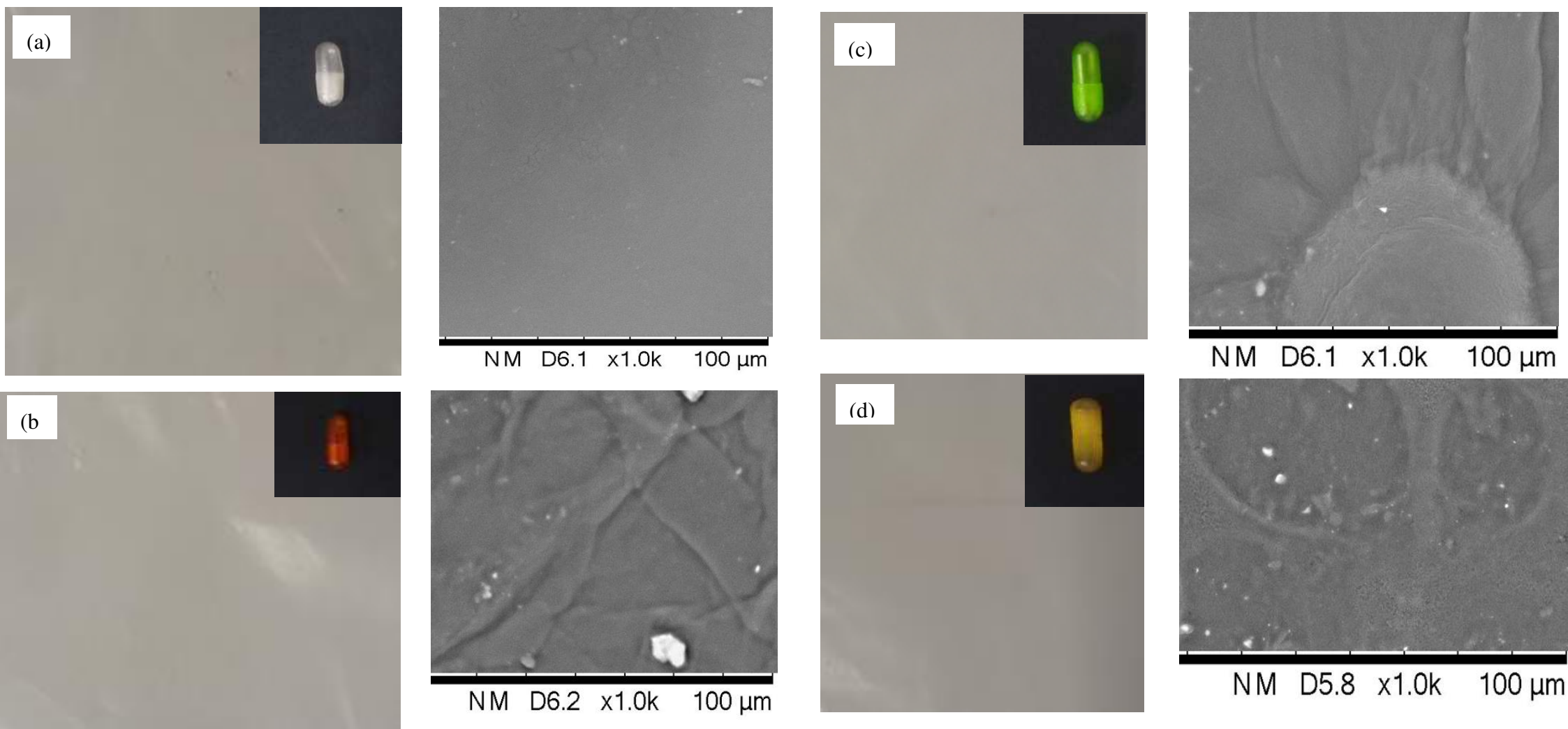


**Figure 6:** Visual representation of Carra-CNCDES biocomposite film and Hard Capsule (a) ratio 1:1 (b) ratio 1:2 (c) ratio 1:3 (d) ratio 1:4.

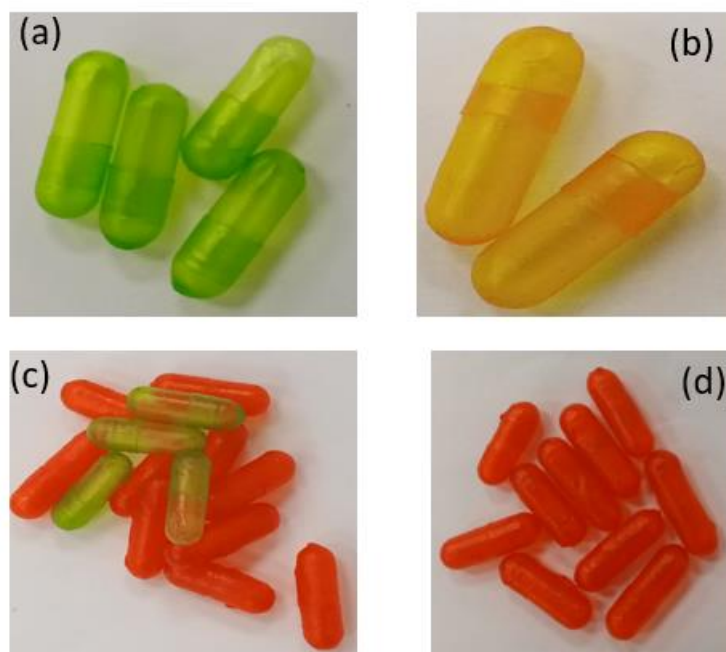


**Figure 7:** Pictorial view of Carra-CNCDES biocomposite film and Hard Capsule (a) ratio 1:1 (b) ratio 1:2 (c) ratio 1:3 (d) ratio 1:4

### **3.9 Comparison of the Properties of Carra-CNCDES Biocomposite and Commercial Gelatin and HPMC Hard Capsule**

The biocomposite films and capsules developed in this study, using various ratios of Carra-CNCDES at 1:1, 1:2, 1:3, and 1:4, mark a significant step forward in sustainable packaging and encapsulation. This compares these new biocomposite capsules with Carra-HPMC, Carra-HPMC/CMSS, Carra-HPMC/CNCDEI formulations, and commercial gelatin and HPMC capsules, as stated in **Table 7**. The mechanical and rheological properties of the Carra-CNCDES capsules, particularly the viscosity, were comparable to those of commercial options, making them suitable for practical use. Viscosity affects processing, filling, and performance, while mechanical properties like tensile strength and elongation at break ensure durability during handling and transportation (Mohammed et al., 2024). By adjusting the HBD in the DES used, the Carra-CNCDES capsules' properties can be tailored for specific applications, whether in pharmaceuticals or nutraceuticals. This flexibility allows customization to meet various needs. Unlike gelatin, which has dietary and allergenic limitations, or HPMC, which is costlier but suitable for vegetarians, Carra-CNCDES capsules

offer a more sustainable and potentially cost-effective option. Using carrageenan, a renewable and biodegradable material, aligns with the push for eco-friendly solutions, reducing dependence on petrochemical plastics. Incorporating CNCDES enhances the material's properties through unique interactions, providing a promising alternative that maintains performance standards (Zdanowicz et al., 2018). This study on the development of Carra-CNCDES biocomposite capsules advances sustainable packaging, offering a practical solution to the issues of plastic waste and environmental impact. With the potential for customization and compatibility with current manufacturing processes, these biocomposites could facilitate a broader transition to sustainable practices in the packaging industry (Mathew et al., 2024). The research underscores the promise of Carra-CNCDES materials in contributing to a more environmentally conscious packaging sector.

**Table 7:** Comparison of the properties of carrageenan biocomposite in current work and commercial gelatin and HPMC Capsules

<b>Tile</b>	<b>Hard Capsules</b>	<b>Viscosity (mPa-s)</b>	<b>Tensile strength (MPa)</b>	<b>Loop strength (N)</b>	<b>Tm (°C)</b>	<b>Ea (KJ/mol)</b>	<b>Moisture content (%)</b>	<b>Disintegration Time (min)</b>	<b>Ref</b>
1.	Carra	172.1	21.0	16.3	66.8	36.6	23.2	10.6	(Al Rizqi Dharma Fauzi et al., 2023)
2.	Carra-HPMC	616.5	51.2	37.4	105.0	64.7	14.6	18.7	(Ramli et al., 2023)
3.	Carra-HPMC/CMSS	738.2	64.5	40.5	74.3	74.4	20.9	16.4	(Ramli et al., 2022b)
4.	Carra-HPMC/CNC DI	704.4	63.8	41.6	80.0	117.1	19.8	4.2	(Ramli, Adam, et al., 2024b)
5.	Gelatin	750-1000	31.0	115.0	187.3	NA	13.0	15.0	(A. M. Smith et al., 2010)
6.	HPMC	1600-2000	19.9	68.9	182.4	NA	4.5	30.0	(Faulhammer et al., 2016)
7.	Carra-CNCDES (1:1)	924.0	83.35	53.95	228.4	75.1	20.2	8.5	This work

<b>Tile</b>	<b>Hard Capsules</b>	<b>Viscosity (mPa-s)</b>	<b>Tensile strength (MPa)</b>	<b>Loop strength (N)</b>	<b>Tm (°C)</b>	<b>Ea (KJ/mol)</b>	<b>Moisture content (%)</b>	<b>Disintegration Time (min)</b>	<b>Ref</b>
8.	Carra-CNCDES (1:2)	1034.0	90.84	69.85	244.3	75.1	19.9	8.0	This work
9.	Carra-CNCDES (1:3)	1219.5	102.04	75.83	245.0	76.8	15.0	7.2	This work
10.	Carra-CNCDES (1:4)	1115.0	89.68	73.22	239.0	79.6	19.3	8.5	This work

## 4 Conclusion

Varying the ratios of HBD to dissolve CNC optimally revealed that a 1:3 ratio of HBD gave a higher breakdown of hydrogen bonds present for 0.2 g of CNC dissolved in 10 g of DES. The resulting 1:3 HBD-reinforced Carra-CNCDES biocomposite film exhibited more thermal stability compared to the ratios of 1:1, 1:2, and 1:4, due to strong intermolecular interactions between CNC and DES, as confirmed by <sup>1</sup>H NMR, XRD, TGA, and FTIR analyses. Reinforcing plant-based materials such as carrageenan enhances the commercial prospects and positions carrageenan-based hard capsules as a superior alternative to gelatine for large-scale production. These biocomposites offer distinct advantages, including environmental friendliness and the potential to meet the growing demand for sustainable materials. However, further studies of mixing methodologies are necessary to address the challenge of rapid solidification, particularly at a standard sample temperature of 60 °C, due to the hydrophilic nature of carrageenan, which will ensure that these hard capsules achieve high quality and can compete with gelatine hard capsules. These advancements will enhance the position of carrageenan hard capsules in the market, by promoting the adoption in drug delivery and other applications where durability and sustainability are crucial.

### ABBREVIATIONS

HBA: Hydrogen Bond Acceptor

HBD: Hydrogen Bond Donor

DES: Deep Eutectic Solvent

ChCl: Choline Chloride

Gly: Glycerol

CNC: Cellulose nanocrystal

<sup>1</sup>H NMR: Proton nuclear magnetic resonance

DMSO-d<sub>6</sub>: Dimethyl Sulfoxide-d<sub>6</sub>

CI: Crystallinity Index

FTIR: Fourier-transform infrared spectroscopy

XRD: X-ray diffraction

TGA: Thermogravimetric analysis

DTG: Derivative of the thermogravimetric

HPMC: Hydroxypropyl methylcellulose

SEM: Scanning electron microscope

## **NOMENCLATURE**

### **Symbols**

Ea: activation energy (kJ/mol)

wt: weight at any time (g)

wo: initial weight (g)

R: universal gas constant ( $\text{mol}^{-1} \text{K}^{-1}$ )

$w_{\infty}$ : weight of residue (g)

T: temperature (K)

Tg: glass transition temperature (C)

A: pre-exponential factor ( $\text{min}^{-1}$ )

Tc: crystallization temperature (C)

Tm: melting temperature (C)

$\Delta H_m$ : melting enthalpy (J/g)

$\Delta H_c$ : crystallization enthalpy (J/g)

$\Delta H$ : enthalpy (kJ/mol)

$\Delta G$ : Gibbs free energy (kJ/mol)

$\Delta S$ : entropy (J/K mol)

### **Dimensionless numbers**

$R^2$  coefficient of determination

y degree of conversion

### **Author contributions**

Chigozie Charity Okwuwa: Conceptualization; writing – original draft; methodology, review, and editing. Fatmawati Adam: Supervision; writing – review and editing. Michael E. Ries: Validation; writing – review and editing.

**Availability of data and materials:** The datasets used and analyzed during the current study are available from the corresponding author upon reasonable request.

**Competing interests:** The authors declare that they have no known competing financial interests or personal relationships that could have appeared to influence the work reported in this paper.

**Funding:** The authors would like to express gratitude to Universiti Malaysia Pahang Al-Sultan Abdullah for funding this work through an internal grant (No: RDU223012).

**Ethics approval:** Not applicable

**Consent to participate:** Not applicable

**Consent for publication:** Not applicable

## References

- Abbasi, N. M., De Silva, S., Biswas, A., & Anderson, J. L. (2023). Ultra-Low Viscosity and High Magnetic Susceptibility Magnetic Ionic Liquids Featuring Functionalized Diglycolic Acid Ester Rare-Earth and Transition Metal Chelates. *ACS Omega*, 8(30), 27751–27760. <https://doi.org/10.1021/acsomega.3c03938>
- Acharya, S., Liyanage, S., Abidi, N., Parajuli, P., Rumi, S. S., & Shamshina, J. L. (2021). Utilization of cellulose to its full potential: A review on cellulose dissolution, regeneration, and applications. In *Polymers* (Vol. 13, Issue 24). MDPI. <https://doi.org/10.3390/polym13244344>
- Adam, F., Jamaludin, J., Abu Bakar, S. H., Abdul Rasid, R., & Hassan, Z. (2020). Evaluation of hard capsule application from seaweed: Gum Arabic-Kappa carrageenan biocomposite films. *Cogent Engineering*, 7(1). <https://doi.org/10.1080/23311916.2020.1765682>
- Ai, W.-T., Su, W.-K., & Su, F. (2023). Solvents Influence <sup>1</sup>H NMR Chemical Shifts and Complete <sup>1</sup>H and <sup>13</sup>C NMR Spectral Assignments for Florfenicol. *Pharmaceutical Fronts*, 05(04), e288–e296. <https://doi.org/10.1055/s-0043-1777285>
- Aiman Hamdan, M., Hikmah Sulaiman, N., Najwa Mohd Amin, K., & Adam, F. (2021). Moisture content and mechanical properties reduction of hard capsules upon prolong drying process. *IOP Conference Series: Materials Science and Engineering*, 1092(1), 012057. <https://doi.org/10.1088/1757-899x/1092/1/012057>
- Al Rizqi Dharma Fauzi, M., Pudjiastuti, P., Hendradi, E., & Teguh Widodo, R. (2023). Development of a potential carrageenan-based hard capsule as the alternative of conventional capsules by implementing the oligomerization reaction. *Journal of Saudi Chemical Society*, 27(4), 101672. <https://doi.org/10.1016/j.jscs.2023.101672>
- Alsoy Altinkaya, S. (2024). A perspective on cellulose dissolution with deep eutectic solvents. *Frontiers in Membrane Science and Technology*, 3. <https://doi.org/10.3389/frmst.2024.1382054>
- Babaei-Ghazvini, A., Vafakish, B., Patel, R., Falua, K. J., Dunlop, M. J., & Acharya, B. (2024). Cellulose nanocrystals in the development of biodegradable materials: A review on CNC resources, modification, and their hybridization. In *International Journal of Biological Macromolecules* (Vol. 258). Elsevier B.V. <https://doi.org/10.1016/j.ijbiomac.2023.128834>
- Bangar, S. P., Harussani, M. M., Ilyas, R. A., Ashogbon, A. O., Singh, A., Trif, M., & Jafari, S. M. (2022). Surface modifications of cellulose nanocrystals: Processes, properties, and applications. *Food Hydrocolloids*, 130, 107689. <https://doi.org/10.1016/j.foodhyd.2022.107689>
- Barani Pour, S., Jahanbin Sardroodi, J., Rastkar Ebrahimzadeh, A., Pazuki, G., & Hadigheh Rezvan, V. (2024). A comparative study of deep eutectic solvents based on fatty acids

- and the effect of water on their intermolecular interactions. *Scientific Reports*, *14*(1), 1763. <https://doi.org/10.1038/s41598-023-50766-1>
- Barros, S. C., da Silva, A. A., Costa, D. B., Cesarino, I., Costa, C. M., Lanceros-Méndez, S., Pawlicka, A., & Silva, M. M. (2014). Thermo-sensitive chitosan–cellulose derivative hydrogels: swelling behaviour and morphologic studies. *Cellulose*, *21*(6), 4531–4544. <https://doi.org/10.1007/s10570-014-0442-9>
- Bashir, I., Dar, A. H., Dash, K. K., Pandey, V. K., Fayaz, U., Shams, R., Srivastava, S., & Singh, R. (2023). Deep eutectic solvents for extraction of functional components from plant-based products: A promising approach. *Sustainable Chemistry and Pharmacy*, *33*, 101102. <https://doi.org/10.1016/j.scp.2023.101102>
- Bisht, B., Kumar, V., Gururani, P., Tomar, M. S., Nanda, M., Vlaskin, M. S., Kumar, S., & Kurbatova, A. (2021). The potential of nuclear magnetic resonance (NMR) in metabolomics and lipidomics of microalgae- a review. In *Archives of Biochemistry and Biophysics* (Vol. 710). Academic Press Inc. <https://doi.org/10.1016/j.abb.2021.108987>
- Calvo-Flores, F. G., & Mingorance-Sánchez, C. (2021). Deep Eutectic Solvents and Multicomponent Reactions: Two Convergent Items to Green Chemistry Strategies. *ChemistryOpen*, *10*(8), 815–829. <https://doi.org/10.1002/open.202100137>
- Cao, B., Du, J., Du, D., Sun, H., Zhu, X., & Fu, H. (2016). Cellobiose as a model system to reveal cellulose dissolution mechanism in acetate-based ionic liquids: Density functional theory study substantiated by NMR spectra. *Carbohydrate Polymers*, *149*, 348–356. <https://doi.org/10.1016/j.carbpol.2016.04.128>
- Cao, J., & Su, E. (2021). Hydrophobic deep eutectic solvents: the new generation of green solvents for diversified and colorful applications in green chemistry. *Journal of Cleaner Production*, *314*, 127965. <https://doi.org/10.1016/j.jclepro.2021.127965>
- Chen, Y., & Mu, T. (2021). Revisiting greenness of ionic liquids and deep eutectic solvents. *Green Chemical Engineering*, *2*(2), 174–186. <https://doi.org/10.1016/j.gce.2021.01.004>
- Cruz, H., Jordao, N., Pinto, A. L., Dionisio, M., Neves, L. A., & Branco, L. C. (2020). Alkaline Iodide-Based Deep Eutectic Solvents for Electrochemical Applications. *ACS Sustainable Chemistry & Engineering*, *9*(9), 9b06733. <https://doi.org/10.1021/acssuschemeng.9b06733>
- Donato, S., Martella, D., Salzano de Luna, M., Arecchi, G., Querceto, S., Ferrantini, C., Sacconi, L., Brient, P. L., Chatard, C., Graillot, A., Wiersma, D. S., & Parmeggiani, C. (2023). The Role of Crosslinker Molecular Structure on Mechanical and Light-Actuation Properties in Liquid Crystalline Networks. *Macromolecular Rapid Communications*, *44*(9). <https://doi.org/10.1002/marc.202200958>
- Farooq, M. Q., Abbasi, N. M., & Anderson, J. L. (2020). Deep eutectic solvents in separations: Methods of preparation, polarity, and applications in extractions and capillary electrochromatography. *Journal of Chromatography A*, *1633*, 461613. <https://doi.org/10.1016/j.chroma.2020.461613>
- Faulhammer, E., Kovalcik, A., Wahl, V., Markl, D., Stelzer, F., Lawrence, S., Khinast, J. G., & Paudel, A. (2016). Multi-methodological investigation of the variability of the

- microstructure of HPMC hard capsules. *International Journal of Pharmaceutics*, 511(2), 840–854. <https://doi.org/10.1016/j.ijpharm.2016.08.005>
- Fauzi, M. A. R. D., Pudjiastuti, P., Wibowo, A. C., & Hendradi, E. (2021). Preparation, Properties and Potential of Carrageenan-Based Hard Capsules for Replacing Gelatine: A Review. *Polymers*, 13(16), 2666. <https://doi.org/10.3390/polym13162666>
- Feng, Y., Liu, G., Sun, H., Xu, C., Wu, B., Huang, C., & Lei, B. (2022). A novel strategy to intensify the dissolution of cellulose in deep eutectic solvents by partial chemical bonding. *BioResources*, 17(3), 4167–4185. <https://doi.org/10.15376/biores.17.3.4167-4185>
- Gaioto, R. C., Dias, M. C. G. C., Ndiaye, P. M., Igarashi-Mafra, L., & Mafra, M. R. (2023). Choline chloride aqueous solution: A thermophysical study. *Fluid Phase Equilibria*, 574, 113903. <https://doi.org/10.1016/j.fluid.2023.113903>
- Gomez, F. J. V., Espino, M., Fernández, M. A., & Silva, M. F. (2018). A Greener Approach to Prepare Natural Deep Eutectic Solvents. *ChemistrySelect*, 3(22), 6122–6125. <https://doi.org/10.1002/slct.201800713>
- Goyal, S., Hernández, N. B., & Cochran, E. W. (2021). An update on the future prospects of glycerol polymers. *Polymer International*, 70(7), 911–917. <https://doi.org/10.1002/pi.6209>
- Guimarães Junior, M., Teixeira, F. G., & Tonoli, G. H. D. (2018). Effect of the nanofibrillation of bamboo pulp on the thermal, structural, mechanical and physical properties of nanocomposites based on starch/poly(vinyl alcohol) blend. *Cellulose*, 25(3), 1823–1849. <https://doi.org/10.1007/s10570-018-1691-9>
- Gundupalli, M. P., Cheenkachorn, K., Chuetor, S., Kirdponpattara, S., Gundupalli, S. P., Show, P. L., & Sriariyanun, M. (2023). Assessment of pure, mixed and diluted deep eutectic solvents on Napier grass (*Cenchrus purpureus*): Compositional and characterization studies of cellulose, hemicellulose and lignin. *Carbohydrate Polymers*, 306. <https://doi.org/10.1016/j.carbpol.2023.120599>
- Gygli, G., Xu, X., & Pleiss, J. (2020). Meta-analysis of viscosity of aqueous deep eutectic solvents and their components. *Scientific Reports*, 10(1), 21395. <https://doi.org/10.1038/s41598-020-78101-y>
- Hamdan, M. A., Khairatun Najwa, M. A., Jose, R., Martin, D., & Adam, F. (2021). Tuning mechanical properties of seaweeds for hard capsules: A step forward for a sustainable drug delivery medium. *Food Hydrocolloids for Health*, 1, 100023. <https://doi.org/10.1016/j.fhfh.2021.100023>
- Hamdan, M. A., Lakashmi, S. S., Mohd Amin, K. N., & Adam, F. (2020). Carrageenan-based hard capsule properties at different drying time. *IOP Conference Series: Materials Science and Engineering*, 736(5). <https://doi.org/10.1088/1757-899X/736/5/052005>
- Hamdan, M. A., Mohd Amin, K. N., & Adam, F. (2024). Quantitative analysis of molecular interactions in  $\kappa$ -carrageenan-Isovanillin biocomposite for biodegradable packaging and pharmaceutical applications using NMR, TOF-SIMS, and XPS approach. *Food Chemistry*, 452. <https://doi.org/10.1016/j.foodchem.2024.139556>

- Hamdan, M. A., Ramli, N. A., Othman, N. A., Mohd Amin, K. N., & Adam, F. (2019). Characterization and property investigation of microcrystalline cellulose (MCC) and carboxymethyl cellulose (CMC) filler on the carrageenan-based biocomposite film. *Materials Today: Proceedings*, 42, 56–62. <https://doi.org/10.1016/j.matpr.2020.09.304>
- Hawkins, J. E., Liang, Y., Ries, M. E., & Hine, P. J. (2021). Time temperature superposition of the dissolution of cellulose fibres by the ionic liquid 1-ethyl-3-methylimidazolium acetate with cosolvent dimethyl sulfoxide. *Carbohydrate Polymer Technologies and Applications*, 2, 100021. <https://doi.org/10.1016/j.carpta.2020.100021>
- Hospodarova, V., Singovszka, E., & Stevulova, N. (2018). Characterization of Cellulosic Fibers by FTIR Spectroscopy for Their Further Implementation to Building Materials. *American Journal of Analytical Chemistry*, 09(06), 303–310. <https://doi.org/10.4236/ajac.2018.96023>
- Jadhav, S., Ganvir, V., Shinde, Y., Revankar, S., Thakre, S., & Singh, M. K. (2021). Carboxylate functionalized imidazolium-based zwitterions as benign and sustainable solvent for cellulose dissolution: Synthesis and characterization. *Journal of Molecular Liquids*, 344. <https://doi.org/10.1016/j.molliq.2021.117724>
- Jančíková, V., & Jablonský, M. (2022). Delignification of Hemp Stalk Using a Low Transition Temperature Mixture Composed of Choline Chloride and Lactic Acid. In *BioResources* (Vol. 17, Issue 1, pp. 1232–1240). North Carolina State University. <https://doi.org/10.15376/biores.17.1.1232-1240>
- Jha, M. K., Malik, A., & Kashyap, H. K. (2023). How hydrogen bond donor acceptor ratio and water content impact heterogeneity in microstructure and dynamics of N,N-diisooctylacetamide and decanol based hydrophobic deep eutectic solvent. *Journal of Molecular Liquids*, 385. <https://doi.org/10.1016/j.molliq.2023.122127>
- Jiang, W.-J., Zhang, J.-B., Zou, Y.-T., Peng, H.-L., & Huang, K. (2020). Manufacturing Acidities of Hydrogen-Bond Donors in Deep Eutectic Solvents for Effective and Reversible NH<sub>3</sub> Capture. *ACS Sustainable Chemistry & Engineering*, 8(35), 13408–13417. <https://doi.org/10.1021/acssuschemeng.0c04215>
- Kalmer, R. R., Haddadan, M. M., Azizi, M., Ghanbari, M., Samandarian, D., Sadjadinia, A., Ramezanalizadeh, H., Karimi, A., & Golizadeh, M. (2023). Industrial Manufacture of Enteric Hard Capsules Using Novel Formulations Based on Hypromellose Phthalate/Gelatin and Investigation of Pantoprazole Release. *ACS Omega*, 8(12), 11293–11303. <https://doi.org/10.1021/acsomega.2c08290>
- Kim, H. U., Kim, J. W., Seo, S., Park, Y.-K., & Jae, J. (2022). *Hydrolysis of Regenerated Cellulose from Ionic Liquids and Deep Eutectic Solvent over Sulfonated Carbon Catalysts*. <https://doi.org/10.21203/rs.3.rs-1916934/v1>
- Kim, S., Nguyen Thi, H., Kang, J., Hwang, J., Kim, S., Park, S., Lee, J.-H., Abdellah, M. H., Szekely, G., Suk Lee, J., & Kim, J. F. (2024). Sustainable fabrication of solvent resistant biodegradable cellulose membranes using green solvents. *Chemical Engineering Journal*, 494, 153201. <https://doi.org/10.1016/j.cej.2024.153201>

- Koch, M., & Włodarczyk-Biegun, M. K. (2020). Faithful scanning electron microscopic (SEM) visualization of 3D printed alginate-based scaffolds. *Bioprinting*, *20*, e00098. <https://doi.org/10.1016/j.bprint.2020.e00098>
- Li, C., Huang, C., Zhao, Y., Zheng, C., Su, H., Zhang, L., Luo, W., Zhao, H., Wang, S., & Huang, L.-J. (2021). Effect of Choline-Based Deep Eutectic Solvent Pretreatment on the Structure of Cellulose and Lignin in Bagasse. *Processes*, *9*(2), 384. <https://doi.org/10.3390/pr9020384>
- Li, L., Ni, R., Shao, Y., & Mao, S. (2014). Carrageenan and its applications in drug delivery. *Carbohydrate Polymers*, *103*, 1–11. <https://doi.org/10.1016/j.carbpol.2013.12.008>
- Li, X., Li, J.-Y., Manzoor, M. F., Lin, Q.-Y., Shen, J., Liao, L., & Zeng, X.-A. (2024). Natural deep eutectic solvent: A promising eco-friendly food bio-inspired antifreezing. *Food Chemistry*, *437*, 137808. <https://doi.org/10.1016/j.foodchem.2023.137808>
- Liang, X., Zhang, J., Huang, Z., & Guo, Y. (2023). Sustainable recovery and recycling of natural deep eutectic solvent for biomass fractionation via industrial membrane-based technique. *Industrial Crops and Products*, *194*. <https://doi.org/10.1016/j.indcrop.2023.116351>
- Liu, Z., Hou, Y., Hu, S., & Li, Y. (2020). Possible dissolution mechanism of alkali lignin in lactic acid-choline chloride under mild conditions. *RSC Advances*, *10*(67), 40649–40657. <https://doi.org/10.1039/d0ra07808e>
- Lomba, L., Ribate, M. P., Sangüesa, E., Concha, J., Garralaga, M. <sup>a</sup> P., Errazquin, D., García, C. B., & Giner, B. (2021). Deep Eutectic Solvents: Are They Safe? *Applied Sciences*, *11*(21), 10061. <https://doi.org/10.3390/app112110061>
- Manafpour, A. A., Feyzi, F., & Rezaee, M. (2024). An environmentally friendly deep eutectic solvent for CO<sub>2</sub> capture. *Scientific Reports*, *14*(1), 19744. <https://doi.org/10.1038/s41598-024-70761-4>
- Marchel, M., Cieśliński, H., & Boczkaj, G. (2022). Thermal Instability of Choline Chloride-Based Deep Eutectic Solvents and Its Influence on Their Toxicity—Important Limitations of DESs as Sustainable Materials. *Industrial & Engineering Chemistry Research*, *61*(30), 11288–11300. <https://doi.org/10.1021/acs.iecr.2c01898>
- Mariano, M., El Kissi, N., & Dufresne, A. (2014). Cellulose nanocrystals and related nanocomposites: Review of some properties and challenges. *Journal of Polymer Science Part B: Polymer Physics*, *52*(12), 791–806. <https://doi.org/10.1002/polb.23490>
- Mohammed, K., Yu, D., Mahdi, A. A., Zhang, L., Obadi, M., Al-Ansi, W., & Xia, W. (2024). Influence of cellulose viscosity on the physical, mechanical, and barrier properties of the chitosan-based films. *International Journal of Biological Macromolecules*, *259*, 129383. <https://doi.org/10.1016/j.ijbiomac.2024.129383>
- Mohd Amin, K. N. (2022). Enhanced thermal stability of cellulose nanocrystals for processing polymer nanocomposites at a high temperature. In *Industrial Applications of Nanocellulose and its Nanocomposites* (pp. 327–335). Elsevier. <https://doi.org/10.1016/B978-0-323-89909-3.00007-9>

- Mohd Amin, K. N., Annamalai, P. K., Morrow, I. C., & Martin, D. (2015). Production of cellulose nanocrystals via a scalable mechanical method. *RSC Advances*, 5(70), 57133–57140. <https://doi.org/10.1039/c5ra06862b>
- Nam, N. N., Do, H. D. K., Trinh, K. T. L., & Lee, N. Y. (2023). Design Strategy and Application of Deep Eutectic Solvents for Green Synthesis of Nanomaterials. *Nanomaterials*, 13(7), 1164. <https://doi.org/10.3390/nano13071164>
- Nandiyanto, A. B. D., Oktiani, R., & Ragadhita, R. (2019). How to read and interpret ftir spectroscopy of organic material. *Indonesian Journal of Science and Technology*, 4(1), 97–118. <https://doi.org/10.17509/ijost.v4i1.15806>
- Nguyen, H. V. D., De Vries, R., & Stoyanov, S. D. (2020). Natural Deep Eutectics as a “Green” Cellulose Cosolvent. *ACS Sustainable Chemistry & Engineering*, 8(37), 14166–14178. <https://doi.org/10.1021/acssuschemeng.0c04982>
- Nguyen, L. N., Vu, M. T., Vu, H. P., Zdarta, J., Mohammed, J. A. H., Pathak, N., Ralph, P. J., & Nghiem, L. D. (2022). Seaweed carrageenans: Productions and applications. In *Algae-Based Biomaterials for Sustainable Development* (pp. 67–80). Elsevier. <https://doi.org/10.1016/B978-0-323-96142-4.00001-4>
- Okwuwa, C. C., Adam, F., Mohd Said, F., & Ries, M. E. (2023). Cellulose dissolution for edible biocomposites in deep eutectic solvents: A review. *Journal of Cleaner Production*, 427. <https://doi.org/10.1016/j.jclepro.2023.139166>
- Omar, K. A., & Sadeghi, R. (2022). Physicochemical properties of deep eutectic solvents: A review. *Journal of Molecular Liquids*, 360, 119524. <https://doi.org/10.1016/j.molliq.2022.119524>
- Omar, K. A., & Sadeghi, R. (2023). Database of deep eutectic solvents and their physical properties: A review. *Journal of Molecular Liquids*, 384, 121899. <https://doi.org/10.1016/j.molliq.2023.121899>
- Pacheco-Quito, E.-M., Ruiz-Caro, R., & Veiga, M.-D. (2020). Carrageenan: Drug Delivery Systems and Other Biomedical Applications. *Marine Drugs*, 18(11), 583. <https://doi.org/10.3390/md18110583>
- Pang, J., Mehandzhyski, A. Y., & Zozoulenko, I. (2023). A computational study of cellulose regeneration: Coarse-grained molecular dynamics simulations. *Carbohydrate Polymers*, 313. <https://doi.org/10.1016/j.carbpol.2023.120853>
- Pelosi, C., Gonzalez-Rivera, J., Bernazzani, L., Tiné, M. R., & Duce, C. (2023). Optimized preparation, thermal characterization and microwave absorption properties of deep eutectic solvents made by choline chloride and hydrated salts of alkali earth metals. *Journal of Molecular Liquids*, 371, 121104. <https://doi.org/10.1016/j.molliq.2022.121104>
- Penner, P., & Vulpetti, A. (2024). QM assisted ML for <sup>19</sup>F NMR chemical shift prediction. *Journal of Computer-Aided Molecular Design*, 38(1). <https://doi.org/10.1007/s10822-023-00542-0>
- Ramírez-Wong, D. G., Ramírez-Cardona, M., Sánchez-Leija, R. J., Rugerio, A., Mauricio-Sánchez, R. A., Hernández-Landaverde, M. A., Carranza, A., Pojman, J. A., Garay-

- Tapia, A. M., Prokhorov, E., Mota-Morales, J. D., & Luna-Bárceñas, G. (2016). Sustainable-solvent-induced polymorphism in chitin films. *Green Chemistry*, 18(15), 4303–4311. <https://doi.org/10.1039/C6GC00628K>
- Ramli, N. A., Adam, F., Mohd Amin, K. N., Abu Bakar, N. F., & Ries, M. E. (2022a). Mechanical and Thermal Evaluation of Carrageenan/Hydroxypropyl Methyl Cellulose Biocomposite Incorporated with Modified Starch Corroborated by Molecular Interaction Recognition. *ACS Applied Polymer Materials*. <https://doi.org/10.1021/acsapm.2c01426>
- Ramli, N. A., Adam, F., Mohd Amin, K. N., Abu Bakar, N. F., & Ries, M. E. (2022b). Mechanical and Thermal Evaluation of Carrageenan/Hydroxypropyl Methyl Cellulose Biocomposite Incorporated with Modified Starch Corroborated by Molecular Interaction Recognition. *ACS Applied Polymer Materials*. <https://doi.org/10.1021/acsapm.2c01426>
- Ramli, N. A., Adam, F., Mohd Amin, K. N., Nor, A. M., & Ries, M. E. (2023). Evaluation of mechanical and thermal properties of carrageenan/hydroxypropyl methyl cellulose hard capsule. *Canadian Journal of Chemical Engineering*, 101(3), 1219–1234. <https://doi.org/10.1002/cjce.24595>
- Ramli, N. A., Adam, F., Ries, M. E., & Ibrahim, S. F. (2024a). DES-ultrasonication treatment of cellulose nanocrystals and the reinforcement in carrageenan biocomposite. *International Journal of Biological Macromolecules*, 270, 132385. <https://doi.org/10.1016/j.ijbiomac.2024.132385>
- Ramli, N. A., Adam, F., Ries, M. E., & Ibrahim, S. F. (2024b). DES-ultrasonication treatment of cellulose nanocrystals and the reinforcement in carrageenan biocomposite. *International Journal of Biological Macromolecules*, 270, 132385. <https://doi.org/10.1016/j.ijbiomac.2024.132385>
- Ramli, N. A., Rosli, F., Aiman Hamdan, M., & Adam, F. (2024). SYNTHESIS OF CARRAGEENAN-BASED BIOCOMPOSITE PLASTICIZED WITH DEEP EUTECTIC SOLVENT AND CHARACTERIZATION OF ITS MECHANICAL PROPERTIES (Sintesis Biokomposit Berasaskan Karaginan Diplastikkan dengan Pelarut Eutektik Dalam dan Penyifatan Ciri-Ciri Mekanikal). In *Malaysian Journal of Analytical Sciences* (Vol. 28).
- Rocky, B. P., & Thompson, A. J. (2021). Characterization of the crystallographic properties of bamboo plants, natural and viscose fibers by X-ray diffraction method. *Journal of the Textile Institute*, 112(8), 1295–1303. <https://doi.org/10.1080/00405000.2020.1813407>
- Sabu Mathew, S., Jaiswal, A. K., & Jaiswal, S. (2024). Carrageenan-based sustainable biomaterials for intelligent food packaging: A review. *Carbohydrate Polymers*, 342, 122267. <https://doi.org/10.1016/j.carbpol.2024.122267>
- Sedayu, B. B., Cran, M. J., & Bigger, S. W. (2020). Reinforcement of refined and semi-refined carrageenan film with nanocellulose. *Polymers*, 12(5). <https://doi.org/10.3390/POLYM12051145>
- Shoab, A. G. M., Ragab, S., El Sikaily, A., Yılmaz, M., & El Nemr, A. (2023). Thermodynamic, kinetic, and isotherm studies of Direct Blue 86 dye absorption by

- cellulose hydrogel. *Scientific Reports*, 13(1). <https://doi.org/10.1038/s41598-023-33078-2>
- Silva, D. A., Webster, G. K., Bou-Chacra, N., & Löbenberg, R. (2018). The Significance of Disintegration Testing in Pharmaceutical Development. *Dissolution Technologies*, 25(3), 30–38. <https://doi.org/10.14227/DT250318P30>
- Sirviö, J. A., Ukkola, J., & Liimatainen, H. (2019). Direct sulfation of cellulose fibers using a reactive deep eutectic solvent to produce highly charged cellulose nanofibers. *Cellulose*, 26(4), 2303–2316. <https://doi.org/10.1007/s10570-019-02257-8>
- Smith, A. M., Ingham, A., Grover, L. M., & Perrie, Y. (2010). Polymer film formulations for the preparation of enteric pharmaceutical capsules. *Journal of Pharmacy and Pharmacology*, 62(2), 167–172. <https://doi.org/10.1211/jpp.62.02.0003>
- Smith, C. J., Wagle, D. V., Bhawawet, N., Gehrke, S., Hollóczki, O., Pingali, S. V., O'Neill, H., & Baker, G. A. (2020). Combined Small-Angle Neutron Scattering, Diffusion NMR, and Molecular Dynamics Study of a Eutectogel: Illuminating the Dynamical Behavior of Glyceline Confined in Bacterial Cellulose Gels. *Journal of Physical Chemistry B*, 124(35), 7647–7658. <https://doi.org/10.1021/acs.jpcc.0c04916>
- Speciale, I., Notaro, A., Garcia-Vello, P., Di Lorenzo, F., Armiento, S., Molinaro, A., Marchetti, R., Silipo, A., & De Castro, C. (2022). Liquid-state NMR spectroscopy for complex carbohydrate structural analysis: A hitchhiker's guide. *Carbohydrate Polymers*, 277. <https://doi.org/10.1016/j.carbpol.2021.118885>
- Sulthan, R., Reghunadhan, A., & Sambhudevan, S. (2023). A new era of chitin synthesis and dissolution using deep eutectic solvents- comparison with ionic liquids. *Journal of Molecular Liquids*, 380, 121794. <https://doi.org/10.1016/j.molliq.2023.121794>
- Sun, H., Zhu, H., Zhu, P., Yang, P., Yu, Z., Zheng, D., Sun, X., Vo, A., Bi, X., Xu, M., & Jiang, F. (2024). Lightweight, mechanically robust and scalable cellulose-based foam enabled by organic-inorganic network and air drying. *Chemical Engineering Journal*, 491, 152014. <https://doi.org/10.1016/j.cej.2024.152014>
- Tamaddon, F., Ahmadi-AhmadAbadi, E., & Noorbala, M. R. (2023). ZnCl<sub>2</sub>:ChCl:2urea as a new ternary deep eutectic for clean production of high content zwitterionic micro- or nano-cellulose by passing to the binary DES of ZnCl<sub>2</sub>:2urea. *Journal of Molecular Liquids*, 387. <https://doi.org/10.1016/j.molliq.2023.122662>
- Tang, F., Li, Y., Huang, J., Tang, J., Chen, X., Yu, H.-Y., Zhou, Y., & Tang, D. (2021). An environmentally friendly and economical strategy to cyclically produce cellulose nanocrystals with high thermal stability and high yield. *Green Chemistry*, 23(13), 4866–4872. <https://doi.org/10.1039/D1GC01392K>
- Thakur, R., Pristijono, P., Scarlett, C. J., Bowyer, M., Singh, S. P., & Vuong, Q. V. (2019). Starch-based films: Major factors affecting their properties. *International Journal of Biological Macromolecules*, 132, 1079–1089. <https://doi.org/10.1016/j.ijbiomac.2019.03.190>
- Thi, S., & Lee, K. M. (2019). Comparison of deep eutectic solvents (DES) on pretreatment of oil palm empty fruit bunch (OPEFB): Cellulose digestibility, structural and morphology

- changes. *Bioresource Technology*, 282, 525–529. <https://doi.org/10.1016/j.biortech.2019.03.065>
- Tong, J., Hu, W., Qin, Y., & Liu, Y. (2023). Deep eutectic solvent pretreatment for green preparation of nanocellulose. In *Cellulose*. Springer Science and Business Media B.V. <https://doi.org/10.1007/s10570-023-05154-3>
- Verma, S., Saini, K., & Maken, S. (2024). Deep eutectic solvents: A long-term approach to chemical synthesis and separation. *Journal of Molecular Liquids*, 393, 123605. <https://doi.org/10.1016/j.molliq.2023.123605>
- Walters, C. M., Boott, C. E., Nguyen, T.-D., Hamad, W. Y., & MacLachlan, M. J. (2020). Iridescent Cellulose Nanocrystal Films Modified with Hydroxypropyl Cellulose. *Biomacromolecules*, 21(3), 1295–1302. <https://doi.org/10.1021/acs.biomac.0c00056>
- Wei, L., Zhang, W., Yang, J., Pan, Y., Chen, H., & Zhang, Z. (2023). The application of deep eutectic solvents systems based on choline chloride in the preparation of biodegradable food packaging films. *Trends in Food Science & Technology*, 139, 104124. <https://doi.org/10.1016/j.tifs.2023.104124>
- Xu, A., & Wang, F. (2020). Carboxylate ionic liquid solvent systems from 2006 to 2020: thermal properties and application in cellulose processing. *Green Chemistry*, 22(22), 7622–7664. <https://doi.org/10.1039/D0GC02840A>
- Yang, F., Zheng, Q., Tan, H., & Wang, X. (2024). Insight into the role of hydrogen bond donor in deep eutectic solvents. *Journal of Molecular Liquids*, 399, 124332. <https://doi.org/10.1016/j.molliq.2024.124332>
- Yang, N., Chen, H., Jin, Z., Hou, J., Zhang, Y., Han, H., Shen, Y., & Guo, S. (2020). Moisture sorption and desorption properties of gelatin, HPMC and pullulan hard capsules. *International Journal of Biological Macromolecules*, 159, 659–666. <https://doi.org/10.1016/j.ijbiomac.2020.05.110>
- Yu, J., Liu, X., Xu, S., Shao, P., Li, J., Chen, Z., Wang, X., Lin, Y., & Renard, C. M. G. C. (2023). Advances in green solvents for production of polysaccharide-based packaging films: Insights of ionic liquids and deep eutectic solvents. *Comprehensive Reviews in Food Science and Food Safety*, 22(2), 1030–1057. <https://doi.org/10.1111/1541-4337.13099>
- Zdanowicz, M., Wilpiszewska, K., & Szychaj, T. (2018). Deep eutectic solvents for polysaccharides processing. A review. *Carbohydrate Polymers*, 200, 361–380. <https://doi.org/10.1016/j.carbpol.2018.07.078>
- Zhang, H., Lang, J., Lan, P., Yang, H., Lu, J., & Wang, Z. (2020). Study on the Dissolution Mechanism of Cellulose by ChCl-Based Deep Eutectic Solvents. *Materials*, 13(2), 278. <https://doi.org/10.3390/ma13020278>
- Zhang, Q., De Oliveira Vigier, K., Royer, S., & Jérôme, F. (2012). Deep eutectic solvents: syntheses, properties and applications. *Chemical Society Reviews*, 41(21), 7108. <https://doi.org/10.1039/c2cs35178a>

